Pharmacokinetic Modeling of Oral siRNA Therapeutics for Treatment of Inflammatory Bowel Disease

Ravali K. Bhavaraju

BME 679H

Engineering Honors Program

The University of Texas at Austin

April 2024

Submitted to:

Nicholas A. Peppas, Sc.D.

Department of Biomedical Engineering

The University of Texas at Austin

Supervising Professor

Andrew Dunn, Ph.D.

Department of Biomedical Engineering

The University of Texas at Austin

Second Reader

ABSTRACT

Author: Ravali Bhavaraju

Title: Pharmacokinetic Modeling of Oral siRNA Therapeutics for Treatment of Inflammatory Bowel Disease

Supervising Professor: Nicholas A. Peppas, Sc. D.

This thesis investigates the pharmacokinetics of orally administered small interfering RNA (siRNA) for the treatment of Inflammatory Bowel Disease (IBD). This study involves the construction of two physiologically based pharmacokinetic (PBPK) models to examine the absorption, distribution, metabolism, and elimination of siRNA across several physiological compartments in the gastrointestinal (GI) tract and within cells.

The first model, the GI transfer PBPK model, examines the pharmacokinetics of siRNA in eight compartments, focusing on the stomach, duodenum, jejunum, ileum, colon, liver, plasma, and kidneys. Key parameters, including compartment volumes, absorption rate constants, and elimination rate constants, were derived from literature and data fitting in MATLAB SimBiology. Sensitivity analyses identified key rate constants, such as the absorption into the stomach, the elimination from the jejunum, and the absorption into the ileum, that significantly influence siRNA concentrations, suggesting critical factors for optimizing IBD treatment.

The second model, the cell PBPK model, examines the intracellular journey of siRNA within target cells in the ileum, focusing on endosomal uptake, cytoplasmic release, and binding to the RNA-induced silencing complex (RISC). Sensitivity analyses on this model indicated that endosomal escape and the association to RISC significantly impact siRNA's gene-silencing potential, suggesting critical points for optimizing therapeutic strategies at the cellular level.

The findings from these models contribute valuable insights into the pharmacokinetics of siRNA, guiding future research and optimization strategies for IBD treatment. Additional pharmacokinetic data, parameter refinement, and experimental validation are essential to enhance the models' accuracy and adaptability, ultimately contributing to improved IBD treatment and the advancement of siRNA-based therapy.

TABLE OF CONTENTS

LIST OF FIGURES AND TABLES

ACKNOWLEDGEMENTS

I would like to thank my supervisor, Dr. Nicholas A. Peppas, for giving me the opportunity to complete this thesis and for his consistent guidance and support throughout the process. His expertise and insights were invaluable to this research. I also want to thank my second reader, Dr. Andrew Dunn, for his feedback and support. I would like to express my gratitude to Ishaan Duggal, my lab mentor, for his assistance with the research and writing process. His guidance was crucial to this project. Finally, I would like to thank my friends and family for their encouragement and support throughout this journey.

CHAPTER 1

INTRODUCTION

1.1 Inflammatory Bowel Disease

Inflammatory bowel disease (IBD) is a set of chronic conditions characterized by inflammation in the gastrointestinal (GI) tract. IBD consists of two major forms, Crohn's disease (CD) and ulcerative colitis (UC). Approximately 3.1 million adults in the United States, representing 1.3% of the adult population, are diagnosed with IBD[1]. IBD is typically diagnosed in young adults, with approximately 25% of patients presenting before the age of 20, but it can affect people of any age[2]. Gender-specific prevalence is observed, with Crohn's disease exhibiting a higher prevalence in women, while ulcerative colitis is more prevalent among men. Additionally, rates of IBD are higher in urbanized regions[2].

Crohn's disease and ulcerative colitis differ in clinical presentation and affect different regions of the GI tract. Crohn's disease involves severe inflammation across the GI tract, from the oral cavity to the anus, and through the GI tract's layers[3]. The affected regions are often not continuous and present in patches. Ulcerative colitis affects continuous regions of the colon and rectum and involves inflammation in the mucosal layer of the GI tract. Common symptoms of both Crohn's disease and ulcerative colitis are diarrhea, abdominal pain, rectal bleeding, anemia, and significant weight loss[3].

Research indicates that IBD may be caused by a combination of genetic heritability and environmental factors (Figure 1)[4]. A study of genome-wide data from over 75,000 patients found an association between 163 autosomal genetic risk loci and IBD[5]. Crohn's disease and ulcerative

colitis share approximately 110 of the 163 risk loci, with many shared between other immune diseases[6]. IBD is also related to environmental factors and has a positive association with urbanized environments[7,8]. Diet largely defines gut microbiota, and Western diets, which are high in fat, refined sugar, and red meat are linked to increased mucosal inflammation[9]. Use of antibiotics and oral contraceptives, increased hygiene practices, elevated stress levels, and early-life microbial exposures have also been associated with an increased risk of developing IBD[10,11].

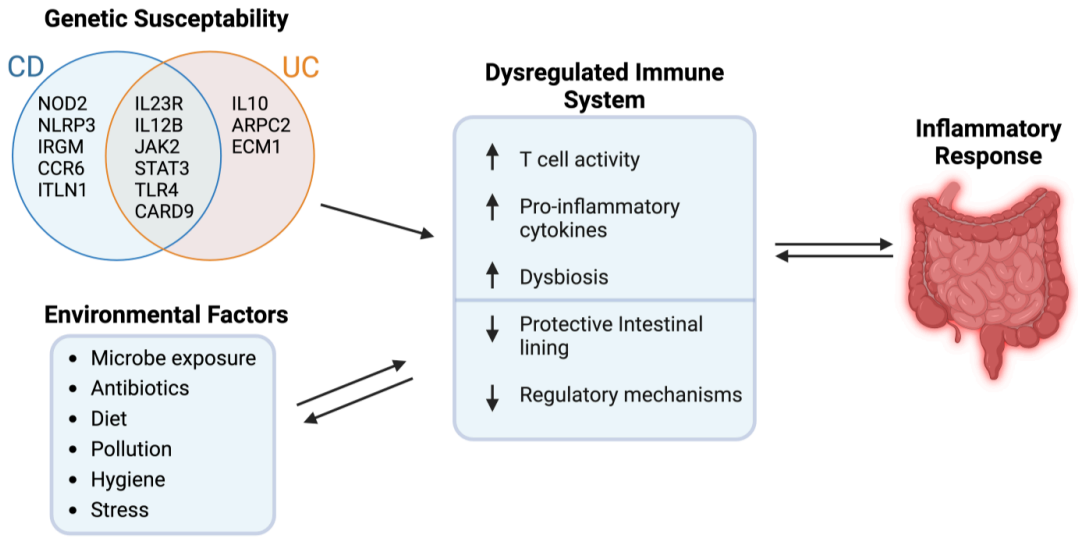

Figure 1 – Interplay of factors involved in IBD pathogenesis. Created with Biorender.com

Pathogenesis of IBD can be described as the result of a dysregulated immune inflammatory state due to genetic factors and an abnormal microbiome[12]. In a dysregulated immune state, epithelial damage is caused by abnormal mucus production and an inability to effectively repair the epithelium[13]. Epithelium damage facilitates the traversal of immune cells, including T cells, B cells, macrophages, and dendritic cells, into the lamina propria[13]. The resulting overproduction of

pro-inflammatory cytokines, such as TNF-α, IL-6, and IL-23, or immune cells, such as T helper cells Th1 and Th17 that produce interleukins, can lead to chronic and sustained immune activation, mucosal disruption, microbial invasion, and tissue damage[12]. Thus, from a molecular point of view, interleukins are a very important factor in the development of the disease.

1.2 Current Treatment Strategies

Current treatments for Inflammatory Bowel Disease include aminosalicylates, corticosteroids, immunomodulators, biologics, and lastly, surgery[14]. Figure 2 depicts a typical progression of treatment for IBD patients.

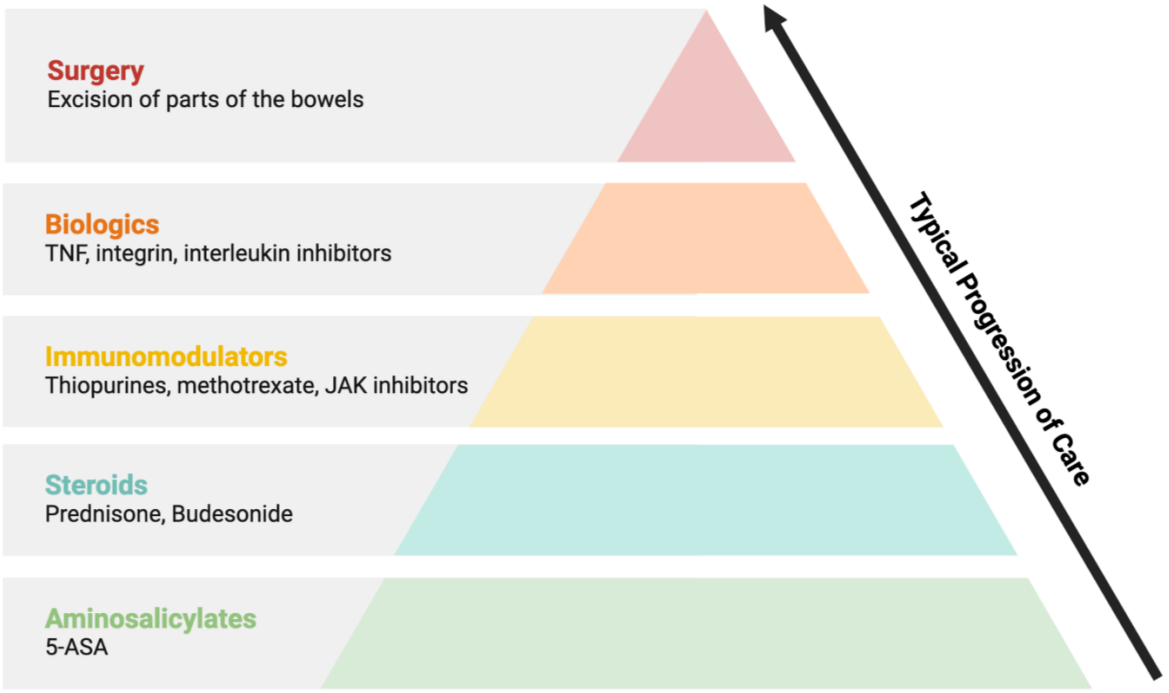

Figure 2 – IBD Treatment Approaches. Created with Biorender.com

Aminosalicylates

5-Aminosalicylates (5-ASA) are therapeutic agents administered to induce remission in patients with mild-to-moderate IBD. It has been reported that from 88 to 97% of patients are prescribed 5-ASA during their first year post-diagnosis[15]. Common 5-ASA-based drugs include sulfasalazine, mesalamine, and olsalazine. 5-ASA reduces inflammation by inhibiting enzymes involved in prostaglandin signaling and the synthesis of inflammatory cytokines such as IL-6 and TNF-α[16]. It also reduces inflammation by blocking reactive oxygen and nitrogen species[17,18].

The therapeutic agent 5-ASA must be formulated in a drug delivery system to target colon mucosa or avoid stomach or small intestine absorption[16]. Common formulations include Asacol, a pH-dependent methacrylic acid-containing copolymer that targets mesalamine delivery to the

ileum and colon, and Pentasa, a semipermeable ethylcellulose membrane that is moisture-sensitive and releases approximately 50% of the drug continuously through the small and large intestines[16,19]. Despite their efficacy in inducing remission and reducing UC relapse, 5-ASA delivery poses a risk of nephrotoxicity, primarily interstitial nephritis[20].

Corticosteroids

Corticosteroids are rapid-acting drugs used to induce remission in patients with moderate-to-severe IBD[16]. Corticosteroids manage inflammation by reducing intestinal permeability, causing apoptosis of lymphocytes, and managing proinflammatory transcription factors, such as NF-κ[16]. Prednisone (PRED) is the most commonly prescribed corticosteroid and has a 50% remission rate[21]. PRED binds to glucocorticoid receptors and reduces the production of proinflammatory prostaglandins and cytokines systemically[21].

While corticosteroids are effective at inducing remission quickly, they have no proven efficacy in long-term remission maintenance and have many adverse effects[14,22]. The long-term effects of corticosteroids include increased infection susceptibility, diabetes mellitus, hypertension, osteoporosis, and adrenal insufficiency. Moreover, approximately 15-40% of patients developed steroid dependency or excess[14]. Corticosteroids continue to be a commonly prescribed option, particularly for pediatric patients, due to their low cost and oral administration.

Immunomodulators

Immunomodulators are typically prescribed due to 5-ASA inefficacy and corticosteroid dependency or resistance. The main types of immunomodulators for IBD are thiopurines,

methotrexate, calcineurin inhibitors, and Janus Kinase (JAK) inhibitors[23]. Thiopurines, such as 6-mercaptopurine, deactivate processes in T lymphocytes that cause inflammation by disturbing nucleic acid synthesis[24,25]. Methotrexate inhibits enzymes, such as AICAR transformylase, causing an accumulation of anti-inflammatory adenosine and down-regulation of immune cells[26]. Calcineurin inhibitors, such as cyclosporine A, interfere with the activation of T cells and inhibit inflammatory cytokines like TNF-α, and IL-2[27]. Lastly, JAK inhibitors inhibit Janus kinases, which bind to cytokine receptors on multiple inflammatory pathways, thereby lowering inflammation[28]. Increased infection susceptibility is a major concern for immunomodulators due to their systemic effects, so screenings for hepatitis B virus, hepatitis C virus, human immunodeficiency virus, and tuberculosis are a common prerequisite to eligibility[16].

Biologics

Biologics provide a targeted form of IBD treatment by inhibiting specific inflammatory molecules and pathways without causing systemic immune suppression. However, biologics still have adverse side effects including a higher risk of infection and reactions at the injection site[29]. The most common biologics for IBD are tumor necrosis factor (TNF) inhibitors, such as adalimumab, which inhibit TNF-α, a pro-inflammatory cytokine that plays a role in several inflammatory signaling pathways[30]. Integrin inhibitors are another class of biologics that prevent integrins, or cell surface transmembrane glycoproteins, from facilitating the binding of leukocytes to the GI tract[31]. The most common integrin inhibited for treatment is α4β7, a glycoprotein that is crucial to leukocyte migration and adhesion in the gut[31]. Lastly, interleukin (IL) inhibitors block pro-inflammatory pathways, reduce inflammation, and enable mucosal healing[32]. Of the most common interleukin inhibitors for IBD,

- Ustekinumab targets IL-12 and IL-23;
- Tocilizumab targets IL-6;
- Secukinumab inhibits IL-17; and
- Dupilumab inhibits IL-14 and IL-13[33].

Disadvantages of Current Treatments

While each established IBD treatment has efficacy in managing symptoms and improving patient outcomes, each has its disadvantages. Aminosalicylates, such as mesalazine, have limited efficacy for moderate to severe cases and can cause side effects such as gastrointestinal discomfort[34]. Corticosteroids are efficacious at providing short-term relief but are not recommended for prolonged use due to adverse effects including osteoporosis, diabetes mellitus, and hypertension. The ability of immunomodulators to successfully lower inflammation through immune suppression also increases infection susceptibility and liver toxicity. Lastly, while biologics are potent and targeted in their inhibition of inflammation, they increase infection risk, are expensive, and often have lowered patient compliance due to administration requiring intravenous or subcutaneous injection[29].

Overall, these therapeutic agents treat the symptoms of IBD by modulating active inflammation and targeting existing proteins or pathways. There remains a need for treatments that target the root cause of IBD while maintaining a high degree of specificity and minimizing systemic adverse effects.

1.3 siRNA Treatments

Small Interfering RNA

Small interfering RNA (siRNA) compounds are double-stranded RNA molecules that are part of the RNA interference pathway, a natural gene regulation mechanism that down-regulates specific genes and mRNA sequences[35]. For therapeutic applications, siRNAs can be engineered to silence disease-specific genes by targeting the mRNA associated with the genes. Once administered, the siRNAs require endosomal uptake and cytoplasmic release to bind to the RNA-induced silencing complex (RISC), which facilitates cleavage of the target mRNA. This process prevents protein translation, achieving gene knockdown and silencing[36].

There are currently five siRNA therapeutic agents with approval by the Food and Drug Administration, all of which target the liver[37]. Patisiran and Vutrisiran are approved for the treatment of transthyretin-mediated amyloidosis, Givosiran is approved for acute hepatic porphyria, Lumasiran is approved for for primary type 1 hyperoxaluria, and Inclisiran is approved for for high cholesterol and cardiovascular disease[38]. Additional siRNA drugs are undergoing clinical trials and focus on ocular, dermal, pulmonary, and renal targets.

For IBD management, siRNA can silence genes that are involved in the immune response and inflammation pathways of the GI tract[39]. Several anti-inflammatory siRNA treatments in pre-clinical or clinical stages target TNF-α, integrins, interleukins, and other molecules implicated in inflammatory pathways[40].

Nanoparticles for Targeted siRNA Delivery

While siRNA is a promising candidate for targeted gene knockdown in IBD, its delivery faces several challenges (Figure 3). Its negative charge, hydrophilicity, and large molecular weight (~13000 g/mol) hinder cell membrane penetration. siRNA is also susceptible to nuclease degradation, particularly by RNAase and phosphatase due to its phosphodiester bond[41]. Immune system interactions and endosomal entrapment further hinder siRNA cellular uptake and release. Furthermore, while oral administration is often preferable due to increased patient compliance and ease of administration, it exposes siRNA to the GI tract's acidic conditions and digestive enzymes. Thus, there is a need for robust siRNA formulations that can survive harsh GI tract conditions, penetrate the intestinal wall and cell membrane, and deliver into the cytoplasm[42].

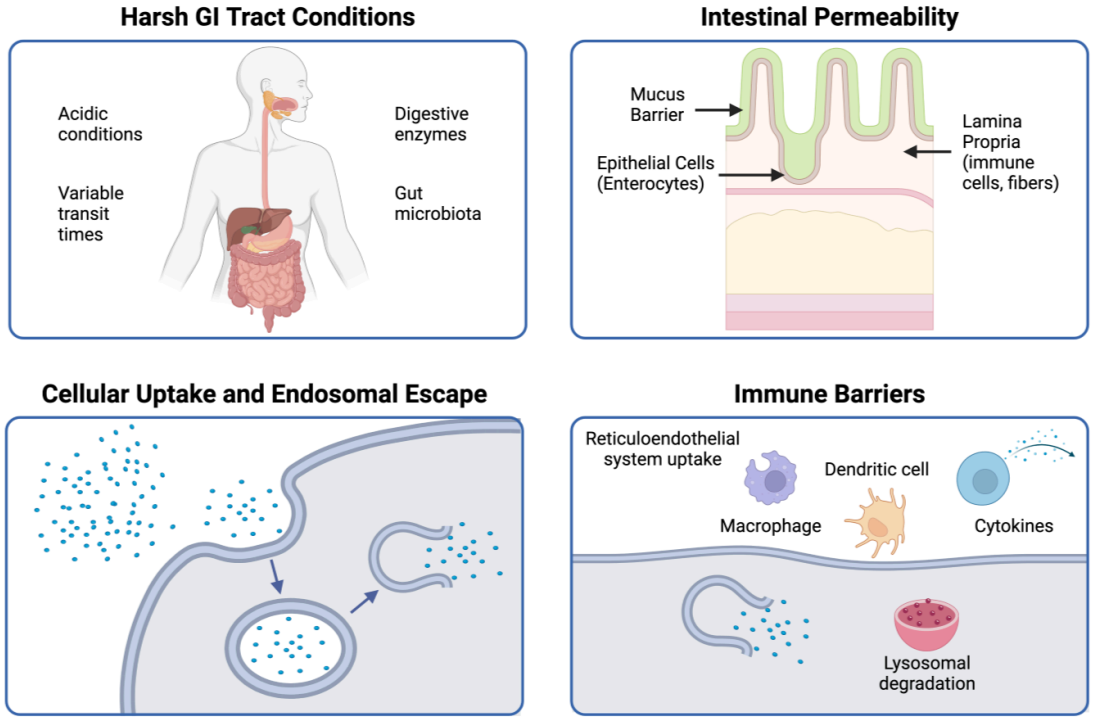

Figure 3 – Barriers to siRNA delivery in the GI tract. Created with Biorender.com

Nanoparticles (NPs) are employed to address these challenges and ensure systemic protection and targeted delivery of siRNA[43]. Nanoparticles are material particles on the nanoscale that are engineered for biological barrier navigation, environmental responsiveness, molecular targeting, and controlled release[44]. For example, hydrophilic NPs can be used to extend circulation time and half-life, while positively charged NPs can be implemented to improve siRNA-NP interaction and cellular uptake.

The three main classes of nanoparticles used in drug delivery are inorganic, polymeric, and lipid-based[45]. Inorganic nanoparticles, including gold or iron-based, are typically used in conjunction with imaging platforms but are less favored due to toxicity and solubility concerns. Polymeric and lipid-based nanoparticles are more prevalent in siRNA delivery[46].

Polymeric NPs are made from natural or synthesized polymers and offer easy modification, biodegradability, and biocompatibility[44]. However, concerns include byproduct toxicity, accumulation, and complex synthesis. Nanocapsules and nanospheres are the most common forms of polymeric NPs[44]. Nanocapsules encapsulate the drug in a polymeric shell, with drug release behavior defined by polymer composition and cross-linking. Due to their enclosed cavities, nanocapsules are preferable over nanospheres for highly lipophilic drugs. In nanospheres, the drug is embedded within the polymer matrix, allowing for uniform and controlled drug release[47].

Lipid-based nanoparticles consist of lipid bilayers enclosing aqueous regions with the therapeutic agent and have high biocompatibility and bioavailability[45]. Liposomes and lipid nanoparticles

(LNPs) are the two forms of lipid-based nanoparticles. Liposomes, composed of one or more phospholipid bilayers, transport hydrophilic and hydrophobic drugs and enhance cellular uptake[48]. Lipid nanoparticles are typically composed of cationic or ionizable lipids, enabling high compatibility with negatively-charged siRNA, enhancing cellular uptake through negatively-charged cell membranes, and improving endosomal escape in the cytoplasm via the proton-sponge effect. Both liposomes and LNPs incorporate cholesterol for structural integrity and cellular uptake and polyethylene glycol (PEG) to evade opsonization and reticuloendothelial system clearance[45].

Several studies have shown the preclinical efficacy of nanoparticle-mediated siRNA therapies for inflammatory GI diseases like IBD. For example, research conducted in Dr. Nicholas A. Peppas' laboratory at The University of Texas at Austin has conducted extensive research in designing hydrogel nanoparticles that can deliver siRNA to the GI tract. These siRNA-loaded nanogels exhibit pH-dependent properties, allowing them to protect siRNA in extracellular environments, deliver specifically to the intestinal area of interest, and release once uptaken into the cell[49–51].

While several studies have shown preclinical efficacy, none have made it further than clinical trials[52]. The most common therapies use oral administration, which enables direct and targeted delivery to the GI tract, reduces systemic exposure, and improves patient compliance[36]. Common siRNA targets for IBD include TNF-α, CD98, Map4k4, IL-22, IL-10, and Cyclin-D1, and effective nanoparticle carriers in studies include liposomes with hyaluronan and DPPE, polyethyleneimine (PEI) derived nanoparticles, calcium phosphate and PLGA nanoparticles,

chitosan-derived nanoparticles, and poly(amino acid) nanoparticles such as poly(lysine) and poly(arginine)[39,40,53].

CHAPTER 2

BACKGROUND

2.1 Pharmacokinetic Modeling

Computational modeling and simulation are used across drug discovery and development to analyze the behavior, efficacy, and safety of therapeutics. These modeling approaches are often used for selecting dosage, planning clinical studies, and supporting regulatory submissions[54]. One important metric examined is *pharmacokinetic (PK) behavior*, which broadly describes how a therapeutic agent is transported through the body[55]. PK models use simplified descriptions of drug movement and physiological processes to describe the concentration of the drug over time, typically in the plasma. Pharmacokinetic/Pharmacodynamic (PK/PD) models correlate a drug's pharmacokinetic profile with its pharmacodynamic (PD) response, which describes the drug's effect on a physiological target[56]. By relating time, drug concentration, and target effect, PK/PD models can create a dose-response curve for a particular drug and disease[54].

Physiologically based pharmacokinetic (PBPK) models can be used to predict pharmacokinetic behavior by modeling the absorption, distribution, metabolism, and elimination (ADME) of a drug in various organs[57]. In PBPK models, the body is divided into compartments that correspond to the different physiological organs in the body, and each compartment is connected by flow rates that correspond to the movement of the drug[58]. The movement of the drug through and between compartments is converted into a series of ordinary differential equations (ODEs) that are solved and describe metrics such as the concentration of the drug in a particular compartment over time[58]. A comprehensive understanding of a drug's pharmacokinetic behavior enables tailoring of the drug to maximize effect and monitor toxicity[55].

The aim of this thesis was to build a physiologically based pharmacokinetic model for oral siRNA therapeutics. This model could provide a better understanding of how an oral siRNA therapeutic travels through the body and can answer questions such as what organs it distributes to, at what rate it moves through them, and how much reaches the target organs.

2.2 Pharmacokinetics of siRNA

Understanding of siRNA pharmacokinetics is rapidly advancing as an increasing number of siRNA therapies are being developed. siRNA has unique pharmacological and chemical properties that affect its ADME characteristics differently from traditional small molecule and biologic-based drugs[54,59]. First, with regards to absorption, small molecules are typically absorbed through diffusion or active transport, and large molecule biologics are absorbed through receptor interaction or lymphatic uptake[60]. siRNA, when conjugated to nanoparticles such as GalNAc, is absorbed through the asialoglycoprotein receptor (ASPGR) and the lymphatic system. Four of the five FDA-approved siRNA treatments, givosiran, lumasiran, inclisiran, and vutisiran, are administered subcutaneously, and the fifth, patisiran, is injected intravenously[60]. Current data shows that siRNA bioavailability is low due to its charge and large size. Inclisiran, for example, had a subcutaneous bioavailability of 24.7-33.8% in monkeys[60,61]. Moreover, after subcutaneous injection, givosiran, lumasiran, inclisiran, and vutisiran were rapidly absorbed and reached peak concentrations between 2 and 4 hours[60].

For distribution, small molecules distribute through diffusion and active transport, and biologic distribution is highly dependent on molecular weight and charge[54,60]. Free siRNA has a short

systemic circulation and can accumulate in the bladder, kidney, and liver, while nanoparticle-conjugated siRNA can be synthesized to distribute mainly to a target organ such as the liver, as occurs with GalNAc conjugates. Because siRNA must distribute into cells to silence genes, interaction with cellular internalization pathways is necessary. For siRNA absorbed into the systemic circulation, balanced plasma protein binding allows for protection from metabolic and clearance pathways while still ensuring adequate tissue distribution[54,60].

In addition, small molecules are metabolized predominantly by cytochrome P450 (CYP) and non-CYP enzymes, and biologics are metabolized by endopeptidases like trypsin. siRNA is subject to nucleolytic, endonuclease, and exonuclease degradation, and mass spectrometry studies have shown free siRNA being metabolized and distributed to tissues at lower molecular weights[62]. These shorter-length oligonucleotide siRNA metabolites can be pharmacologically active, as is the case with givosiran and its active metabolite AS(N-1)3' givosiran. When complexed with nanoparticles, siRNA shows a longer half-life in the plasma and lower plasma clearance than free siRNA[62].

Fourth, small molecules, biologics, and siRNA are eliminated through renal clearance and biliary excretion. Free siRNA and nanoparticle-conjugated siRNA can have highly distinct elimination half-lives, such as 10 minutes for free siRNA and 162 hours for a siRNA/LNP complex[62]. In addition to this, siRNA and components of RISC can be recycled, and 70% of LNP-delivered siRNA has been found to undergo exocytosis due to recycling pathways regulated by Niemann-Pick type C1 (NPC1)[54,63].

The current research on siRNA pharmacokinetics is primarily based on intravenous and subcutaneous administration. There remains a need to find pharmacokinetic data based on oral administration of siRNA for accurate pharmacokinetic modeling.

2.3 Studies on Oral siRNA Pharmacokinetics

Several previous studies have recorded pharmacokinetic data after oral administration of siRNA in vivo. In a 2020 study by Attarwala et al., siRNA was orally administered to C57BL/6 mice to knock down the TG2 gene, which is overexpressed in celiac disease[64]. The siRNA used in this study was encapsulated in two distinct nanoparticle systems. In the first, siRNA was enclosed in type-B gelatin nanoparticles, which were then enclosed in poly(e-caprolactone)-based microspheres. In the second, siRNA was enclosed in type-B gelatin nanoparticles, which were then placed in a safflower oil-based emulsion. The gelatin nanoparticles offered protection from nuclease degradation, while the second hydrophobic encapsulation offered protection from proteases and the low pH of the GI tract. This study included pharmacokinetic profiles of both nanoparticle systems over 96 hours after oral administration of a single dose. It included data in 9 physiological compartments: ileum, colon, duodenum, jejunum, liver, plasma, kidney, stomach, and spleen.

In a 2014 study by Han et al., siRNA was orally administered to tumor-bearing nude mice to knock down the vascular endothelial growth factor (VEGF) gene and treat hepatoma[65]. siRNA labeled with Tetramethylrhodamine (TAMRA) fluorescence was encapsulated in galactose-modified trimethyl chitosan-cysteine (GTC) at varying grafting densities, or ratios of chitosan and lacobionic acid. The trimethyl and cysteine groups improve mucoadhesion through

electrostatic interactions and disulfide bonding, and they improve intestinal permeation through tight junction opening. The galactose modification promoted endocytosis by interacting with asialoglycoprotein receptors (ASPGR) on cancerous hepatocytes. The study included distribution profiles in the plasma, intestine, tumor, heart, liver, kidney, lung, and spleen over 24 hours after oral administration of a single dose.

In a 2017 study by Kang et al., siRNA was administered orally to BALB/c albino mice to target the AKT2 gene for the treatment of colorectal liver metastases (CLM)[66]. The AKT2 siRNA was combined with citrate-stabilized gold nanoparticles to form AuNP-siRNA (AR) complexes, which were then encapsulated in glycol chitosan-taurocholic acid (GT) to form AR-GT complexes. The cationic glycol chitosan protects the therapeutic agent through GI transit, and the taurocholic acid ligands enhance the targeting of colorectal liver metastases by interacting with apical sodium bile acid transporters and promoting movement through the enterohepatic recycling system. This study tracked gold in the AR-GT complexes and recorded nanoparticle accumulation in the stomach, duodenum, jejunum, ileum, liver, kidney, and spleen over 48 hours after oral administration of a single dose.

2.4 Pharmacokinetic Modeling Software

A multitude of software and tools are available to facilitate pharmacokinetic and pharmacodynamic modeling, including MATLAB, GastroPlus, Berkeley Madonna, R, NONMEM, SAAM II, and Simcyp[67–69]. This project uses MATLAB SimBiology, which is an application within MATLAB, a programming and computing environment developed by MathWorks[70]. SimBiology is a modeling and simulation tool for biological systems and is

commonly used for pharmacokinetic and pharmacodynamic analysis. SimBiology's Model Builder tool has a graphical user interface that allows users to construct compartmental models using block diagrams. These diagrams include nodes and links, reflecting physiological compartments and drug flow, respectively[67]. This process automatically generates the underlying ordinary differential equations that describe the system's dynamics. Additionally, the Model Analyzer tool within SimBiology provides a multitude of functionalities, including model simulation, non-compartmental analysis, and sensitivity analysis.

MATLAB SimBiology connects with MATLAB's main Integrated Development Environment (IDE) to combine coding, debugging, and visualization capabilities in one platform. This enables exporting and additional analysis of pharmacokinetic data simulated through the tool. SimBiology also offers flexibility in defining PBPK models[69]. Users can tailor equations and parameters to align with specific research needs. Moreover, MATLAB has advanced computing power and capabilities that are beneficial for PBPK modeling, which often involves complex differential equations with multiple time scales. Overall, MATLAB SimBiology's user interface, flexibility, and computing capabilities make it an effective choice for PBPK modeling.

CHAPTER 3

OBJECTIVES

The goal of this thesis was to build a physiologically based pharmacokinetic (PBPK) model that describes the absorption, distribution, metabolism, and elimination of orally administered siRNA for the treatment of Inflammatory Bowel Disease (IBD). To accomplish this, several specific objectives have been set:

1. To conduct a literature search for existing pharmacokinetic data from in vivo studies of orally-delivered siRNA

2. To construct and solve a PBPK model for orally administered siRNA

3. To perform a sensitivity analysis of the PBPK model and examine the pharmacokinetic response to adjustments in model properties

CHAPTER 4

METHODS

4.1 Extraction of In Vivo Pharmacokinetic Data

The first step to building a pharmacokinetic model of orally administered siRNA was to find pharmacokinetic data in the literature that could be used to calculate model parameters, such as compartmental volumes and flow rates. Among the three studies that documented pharmacokinetic data after the in vivo oral administration of siRNA — Attarwala et al.[64], Han et al.[65], and Kang et al.[66] — the study by Attarwala et al. was selected for parameter estimation.

We preferred to use the study by Attarwala et al. over the studies by Han et al. and Kang et al. for several reasons. The Attarwala et al. study has data points for 96 hours, while the study by Han et al. was completed over 24 hours, and the study by Kang et al. over 48 hours[64–66]. Given that formulations of siRNA and nanoparticles can exhibit half-lives over 90 hours, a longer measurement period would enhance pharmacokinetic study[71]. Additionally, the Attarwala et al. study delineated detailed sections of the intestine — specifically, the duodenum, jejunum, ileum, and colon — while Han et al. presented the intestine as one compartment, and Kang, et al. omitted the colon. Furthermore, Attarwala et al. directly measured and recorded siRNA concentration. On the other hand, Han et al. recorded siRNA distribution percentage, which necessitates further transformation to derive concentration values, thereby introducing the potential for data distortion. Similarly, the Kang et al. methodology estimated siRNA accumulation indirectly through the accumulation of gold, one component of the nanoparticle conjugate. The assumption that accumulation of gold is equal to siRNA accumulation introduces potential inaccuracies that may arise if the gold component behaves differently than siRNA.

Finally, the therapeutic target of siRNA in the Attarwala et al. study is Celiac disease, an inflammatory gastrointestinal disease that aligns closely with the intestinal focus of IBD. The Han et al. study, which targets hepatoma, and the Kang et al. study, which targets colorectal liver metastases, both target the liver rather than the intestines.

The data presented in the Attarwala study were concentration-time profiles of siRNA in the ileum, colon, duodenum, jejunum, liver, plasma, kidney, stomach, and spleen after oral administration of siRNA enclosed in two nanoparticle systems: a Nanoparticle in Microsphere Oral System (NiMOS) and a Nanoparticle in Emulsion (NiE).

WebPlotDigitizer, a computer vision software used for data retrieval from images, was used to extract quantitative data from each compartmental concentration-time plot (Figure 4). WebPlotDigitizer generates the numerical values of selected data points following user definition of reference points on each axis. For the Attarwala pharmacokinetic data, the logarithmic scale of the y-axis was specified as well. Following the application of WebPlotDigitizer, the software generated downloadable .csv files containing the numerical data for each plot point. Because the image data from the NiE nanoparticle system plot was indistinct in several compartments, only the NiMOS system concentration-time profiles were extracted.

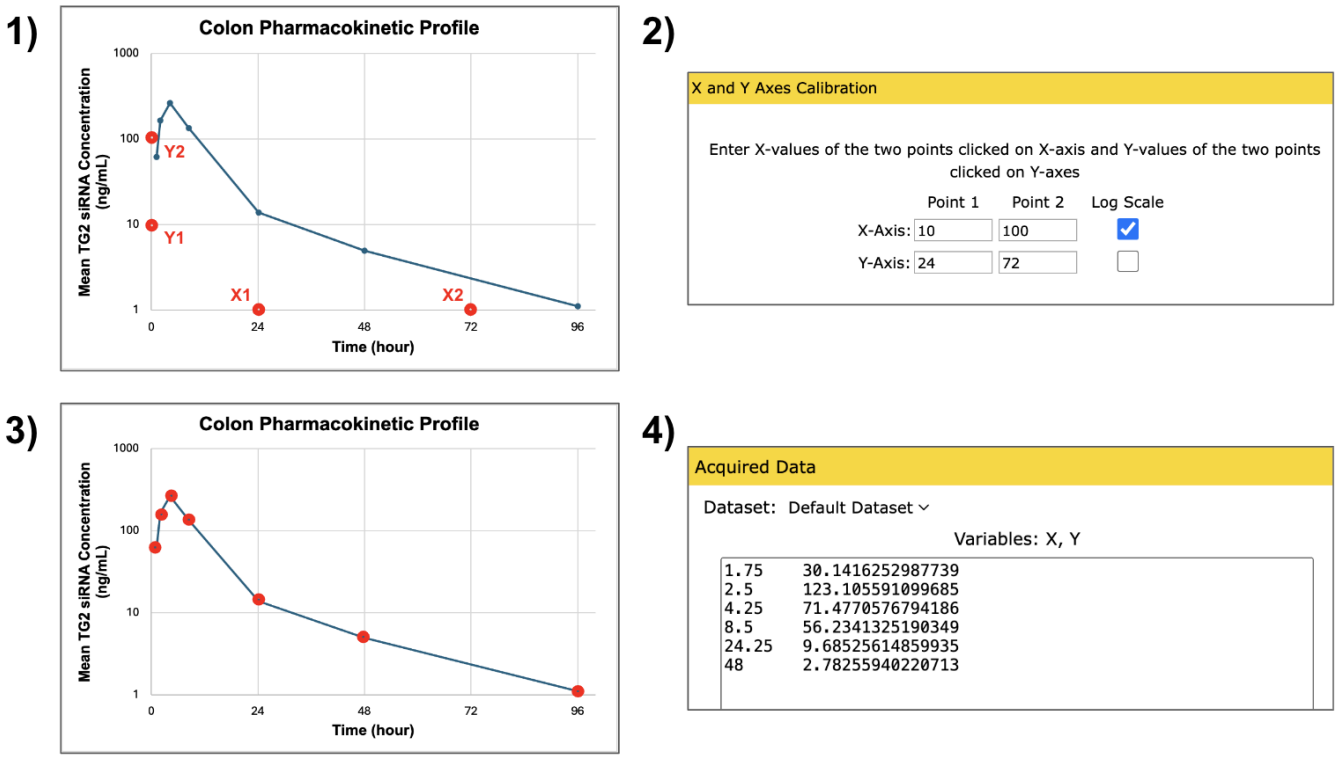

Figure 4 – Example workflow of using WebPlotDigitizer to extract concentration-time data from pharmacokinetic plots. **1)** User clicks four known points on the axes of the plot: two on the x-axis and two on the y-axis. **2)** User enters the known values of the specified points and indicates the scale if applicable. **3)** User clicks on each point that numeric extraction is required for. **4)** WebPlotDigitizer provides the numerical values of each selected point.

4.2 Pharmacokinetic Parameter Estimation

The parameters required for each compartment of the model were the compartment volume, the drug absorption rate into the compartment, and the drug elimination rate from the compartment. The compartment volumes were acquired from studies involving mice of comparable weights to Attarwala et al., which used mice between 20 and 30 grams. The liver and kidney volumes were sourced from Hall et al., the duodenum, jejunum, ileum, and colon volumes were from Casteleyn

et al., the stomach volume was from McConnell et al., and the plasma volume was from Shah et al[72–75].

The absorption and elimination rates for each compartment were estimated from the concentration-time profiles from Attarwala et al. in two steps. First, the *Non-Compartmental Analysis (NCA)* function in the Model Analyzer of MATLAB SimBiology was run with the concentration-time profile data from each compartment (Figure 5). Non-compartmental analysis (NCA) computes pharmacokinetic parameters from concentration-time profiles without the specification of a compartmental model and while assuming linear pharmacokinetics[76]. The NCA results included *CL*, the total drug clearance, and *V_z*, the volume of distribution during the terminal phase. The K_e, or the elimination rate, was calculated by dividing *CL* by *V_z*[77].

A)

DATA

DATA

Duodenum_Data

Save the data with the program results. This must be checked for reports to include the data information.

NCA

DESCRIPTION

Click to edit the description

DEFINITION

Classification	Column
Group	Var1
ID	
Time	Time_hr_
Concentration	Concentration_ng_mL_
IV Bolus Dose	Dose_ng_
Extravascular Dose	

B)

Duodenum_NCA: LastRun: results

	Var1	doseSchedule	administrationRoute	Lambda_Z	CL	DM	V_z
1	1	Single	IVBolus	0.0867	14.5670	12500	168.0731

Figure 5 – Example workflow for running *Non-Compartmental Analysis* on MATLAB SimBiology for calculating initial estimates of compartment volume and elimination rate. **A)** The selected concentration-time profile is added, and profile data is classified into group, time, concentration, and dose. **B)** The results of running *Non-Compartmental Analysis* include estimates of *CL*, the total drug clearance, and *V_z*, the volume of distribution during the terminal phase.

Second, the *Fit Data* function within the Model Analyzer was used to estimate the absorption and elimination rates of each compartment using the results of the NCA as initial estimates (Figure 6). This estimation was run for each of the compartmental concentration-time profiles. The *OneComp with* K_e, or one-compartment with elimination rate, model type was selected. The time data was set as the *independent* class, the concentration data was set as the *response* class, and the dose was defined as an instant bolus dose to the central compartment. The elimination rate, K_e, and volume of distribution, *V_z*, from the NCA were set as the initial untransformed estimates of the central compartment volume and elimination rate, respectively. The nonlinear

least-squares solver, or *lsqnonlin*, was the estimation method used for fitting data. The *Fit Data* function resulted in estimations and standard errors for the compartment volume, *central*, the elimination rate, K_e, and the absorption rate, K_a.

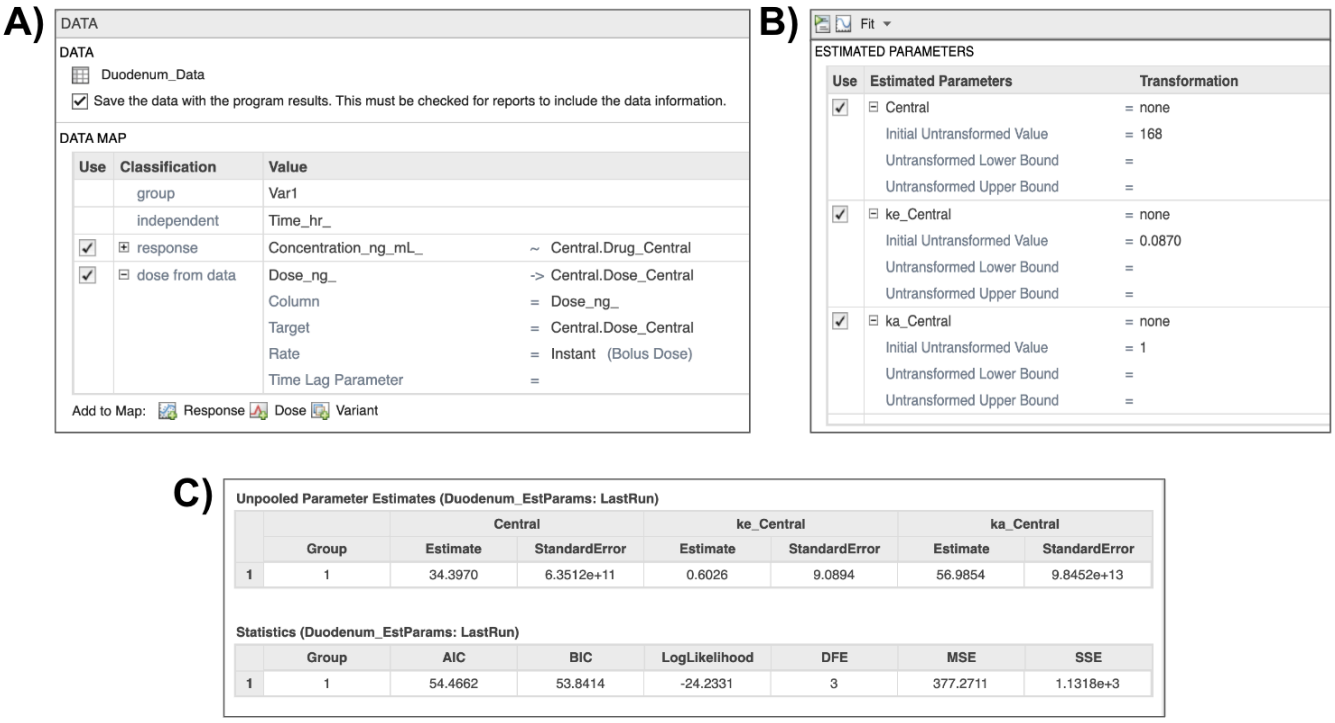

Figure 6 – Example workflow for running *Fit Data* on MATLAB SimBiology for calculating parameter estimates. **A)** The selected concentration-time profile is added, and profile data is classified into group, independent variable, response, and dose. **B)** The results from the non-compartmental analysis are added as initial values for the parameter estimation. **C)** The results of running *Fit Data* include estimates of compartment volume, elimination rate, and absorption rate with statistical estimates for the fit.

4.3 Gastrointestinal Transfer PBPK Model Creation

The SimBiology Model Builder tool was used to build the compartmental model schematic. The Model Builder tool allows users to create block diagram PBPK schematics by adding, defining, and connecting compartment, species, and reaction blocks. The model incorporates eight

compartments: the stomach, duodenum, jejunum, ileum, colon, liver, plasma, and kidneys. Reaction blocks were added between each compartment to indicate flow between compartments and out of each compartment to indicate elimination. A species block was added within each compartment to represent the amount of drug in that compartment and at the end of each elimination rate to represent the amount of drug eliminated out of each compartment.

The compartment volumes derived from literature and the rates estimated in SimBiology were added to define each compartment and reaction, respectively. The absorption rate constants (Ka) were applied to the reaction blocks that went into each compartment from its predecessor. The elimination rate constants (Ke) were applied to the reaction blocks that exited each compartment without subsequent entry into another compartment.

4.4 Cell PBPK Model Creation

A second PBPK model was developed to describe siRNA movement and delivery within the cell. Similar to the primary PBPK model, this cell PBPK model was created using the Model Builder tool in SimBiology. The model was created with the physiological compartments most relevant to siRNA movement within the cell: the endosome, the cytoplasm, and the RISC complex.

Moreover, kinetic rate constants governing siRNA cellular dynamics for this model were adopted from several siRNA cellular kinetics studies. The rate constants for degradation of endosomal siRNA, degradation of free cytoplasmic siRNA, dissociation of siRNA to the RISC complex, and degradation of RISC-loaded siRNA were acquired from a study by Ayyar et al. on the delivery of GalNAc-conjugated siRNA to the hepatic cells of mice[78]. The rate constant for association of

siRNA to the RISC complex was drawn from Ayyar et al. as well. However, because the association rate constant had units of $nM^{-1}hr^{-1}$, it was incompatible with the other rate constants used in the model, which had units of hr^{-1}. Thus, for model compatibility, the rate constant for association of siRNA to RISC from was assumed to follow hr^{-1} units. The rate constant for endosomal escape of siRNA was from a study by Bartlett et al. on in vitro delivery of siRNA to mammalian cells[79]. Lastly, the rate constant for endosomal uptake of siRNA in the ileum was assumed to be 1.

4.5 Model Assumptions

Several key assumptions were used in the development of these models.

1) All pharmacokinetic processes are assumed to follow first-order kinetics, meaning the rates do not saturate at any point.
2) The volumes of each compartment in the GI transfer PBPK model are assumed to be constant throughout the study period.
3) The GI transfer PBPK model only includes the eight specified compartments: the stomach, duodenum, jejunum, ileum, colon, liver, plasma, and kidneys. This assumes these compartments represent the critical sites of siRNA movement and that other tissue interactions are either negligible or have a minor effect.
4) The GI transfer PBPK model assumes that perfusion rates across different compartments are uniform.
5) The cell PBPK model assumes that the initial dose to the endosome is given as a single, instant bolus derived from the siRNA concentration in the ileum.

6) To ensure compatibility in the cell PBPK model, the rate of association of siRNA to the RISC complex is assumed to follow hr^{-1} units instead of the original $nM^{-1}hr^{-1}$ units from Ayyar et al.
7) In the cell PBPK model, the rate of endosomal uptake of siRNA in the ileum is assumed to be 1.
8) The cell PBPK model assumed that only free siRNA in the cytoplasm will associate to the RISC complex.

CHAPTER 5

RESULTS AND DISCUSSION

5.1 Gastrointestinal Transfer PBPK Model

A gastrointestinal (GI) transfer PBPK model was proposed to describe the pharmacokinetics of orally administered siRNA for the treatment of IBD. The compartmental model proposed for this is shown in Figure 7. Each compartment was defined by a compartment volume, absorption rate constant, and elimination rate constant, and all parameters used are defined in Table 1. The model includes eight compartments. Oral administration of the dose is represented by a dose delivered to the first compartment of the model, the stomach, at the start of the simulation. From the stomach, the model splits the intestine into its three parts: the duodenum, the jejunum, and the ileum. The ileum splits into the liver and the colon, which feeds back into the liver. After the liver, the drug enters circulation in the plasma compartment and, lastly, goes through the kidney.

There are eight ordinary differential equations that describe this PBPK model:

$$\frac{dC_{Stomach}}{dt} = k_1 * C_{Dose} - k_2 * C_{Stomach} - k_3 * C_{Stomach}$$

$$\frac{dC_{Duodenum}}{dt} = k_3 * C_{stomach} - k_4 * C_{Duodenum} - k_5 * C_{Duodenum}$$

$$\frac{dC_{Jejunum}}{dt} = k_5 * C_{Duodenum} - k_6 * C_{Jejunum} - k_7 * C_{Jejunum}$$

$$\frac{dC_{Ileum}}{dt} = k_7 * C_{Jejunum} - k_8 * C_{Ileum} - k_9 * C_{Ileum} - k_{11} * C_{Ileum}$$

$$\frac{dC_{Colon}}{dt} = k_9 * C_{Ileum} - k_{10} * C_{Colon} - k_{11} * C_{Colon}$$

$$\frac{dC_{Liver}}{dt} = k_{11} * C_{Ileum} + k_{11} * C_{Colon} - k_{12} * C_{Liver} - k_{13} * C_{Liver}$$

$$\frac{dC_{Plasma}}{dt} = k_{13} * C_{Liver} - k_{14} * C_{Plasma} - k_{15} * C_{Plasma}$$

$$\frac{dC_{Kidney}}{dt} = k_{15} * C_{Plasma} - k_{16} * C_{Kidney}$$

where, $k_1 = k_{absorption,\ stomach}$, $k_2 = k_{elimination,\ stomach}$, $k_3 = k_{absorption,\ duodenum}$, $k_4 = k_{elimination,\ duodenum}$, $k_5 = k_{absorption,\ jejunum}$, $k_6 = k_{elimination,\ jejunum}$, $k_7 = k_{absorption,\ ileum}$, $k_8 = k_{elimination,\ ileum}$, $k_9 = k_{absorption,\ colon}$, $k_{10} = k_{elimination,\ colon}$, $k_{11} = k_{absorption,\ liver}$, $k_{12} = k_{elimination,\ liver}$, $k_{13} = k_{absorption,\ plasma}$, $k_{14} = k_{elimination,\ plasma}$, $k_{15} = k_{absorption,\ kidney}$, and $k_{16} = k_{elimination,\ kidney}$

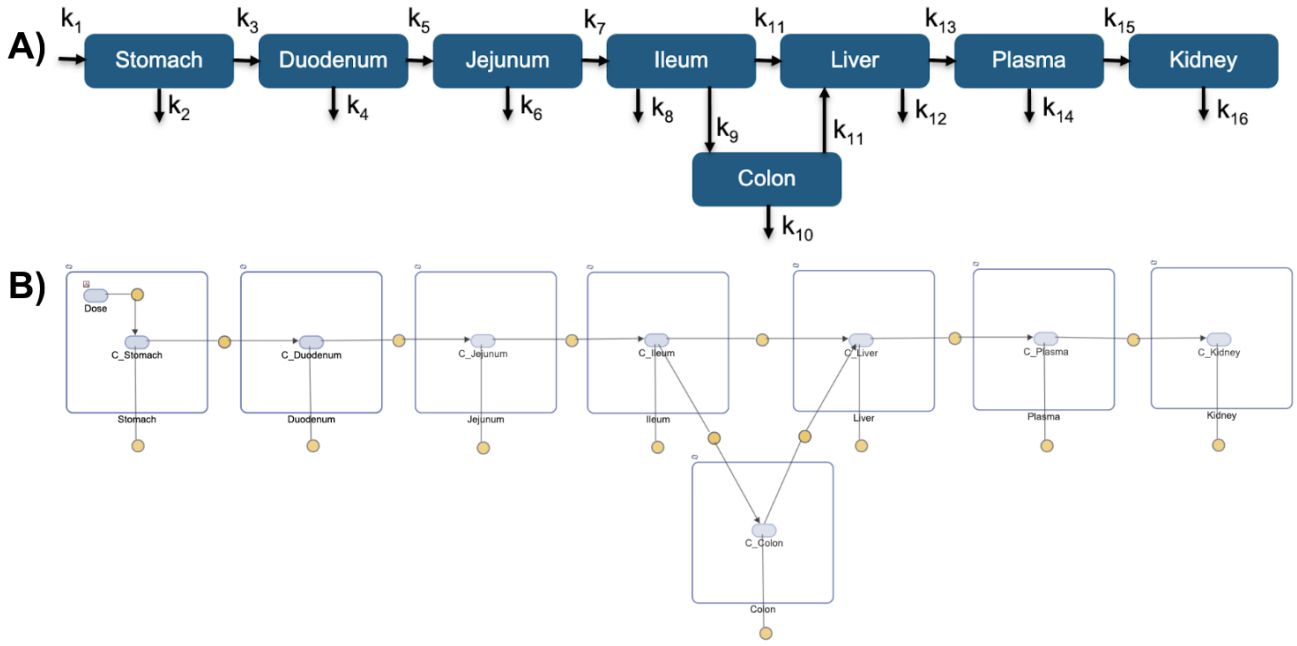

Figure 7 – GI Transfer PBPK Model Schematic. The model includes eight compartments: Stomach, Duodenum, Jejunum, Ileum, Colon, Liver, Plasma, and Kidney. All compartments are defined by rate constants.

Table 1 – GI Transfer PBPK Model Compartment Volumes. All volumes were acquired from literature[73–75].

Parameter	Volume (mL)
$V_{stomach}$	0.37
$V_{duodenum}$	0.21
$V_{jejunum}$	0.69
V_{ileum}	0.07
V_{colon}	0.21
V_{liver}	1.65
V_{plasma}	1
V_{kidney}	0.51

Table 2 – GI Transfer PBPK Model Absorption and Elimination Rates. All rate constants were calculated using the *Fit Data* tool in MATLAB SimBiology and Attarwala et al[64].

Parameter	Description	Rate (hr^{-1})
k_1	$k_{absorption,\ stomach}$	0.1
k_2	$k_{elimination,\ stomach}$	0.5
k_3	$k_{absorption,\ duodenum}$	56.985
k_4	$k_{elimination,\ duodenum}$	0.6026
k_5	$k_{absorption,\ jejunum}$	42.46
k_6	$k_{elimination,\ jejunum}$	13
k_7	$k_{absorption,\ ileum}$	0.3676
k_8	$k_{elimination,\ ileum}$	0.3676

k_9	$k_{absorption,\ colon}$	0.6917
k_{10}	$k_{elimination,\ colon}$	0.01
k_{11}	$k_{absorption,\ liver}$	0.1621
k_{12}	$k_{elimination,\ liver}$	0.01
k_{13}	$k_{absorption,\ plasma}$	0.3567
k_{14}	$k_{elimination,\ plasma}$	0.01
k_{15}	$k_{absorption,\ kidney}$	0.4
k_{16}	$k_{elimination,\ kidney}$	0.5962

The model was simulated with an initial dose of 12500 nanograms to replicate the conditions used in the original study by Attarwala et al. This dose was introduced into the first compartment – the stomach – to mimic oral administration. The simulation results, displayed in Figure 11, show the siRNA concentration across eight compartments over time. The maximum concentration (C_{max}) and the area under the curve (AUC) for each compartment are summarized in Table 3. According to these findings, the highest C_{max} and AUC values are found in the ileum and colon compartments. This outcome is promising, as IBD primarily affects the ileum and colon[80].

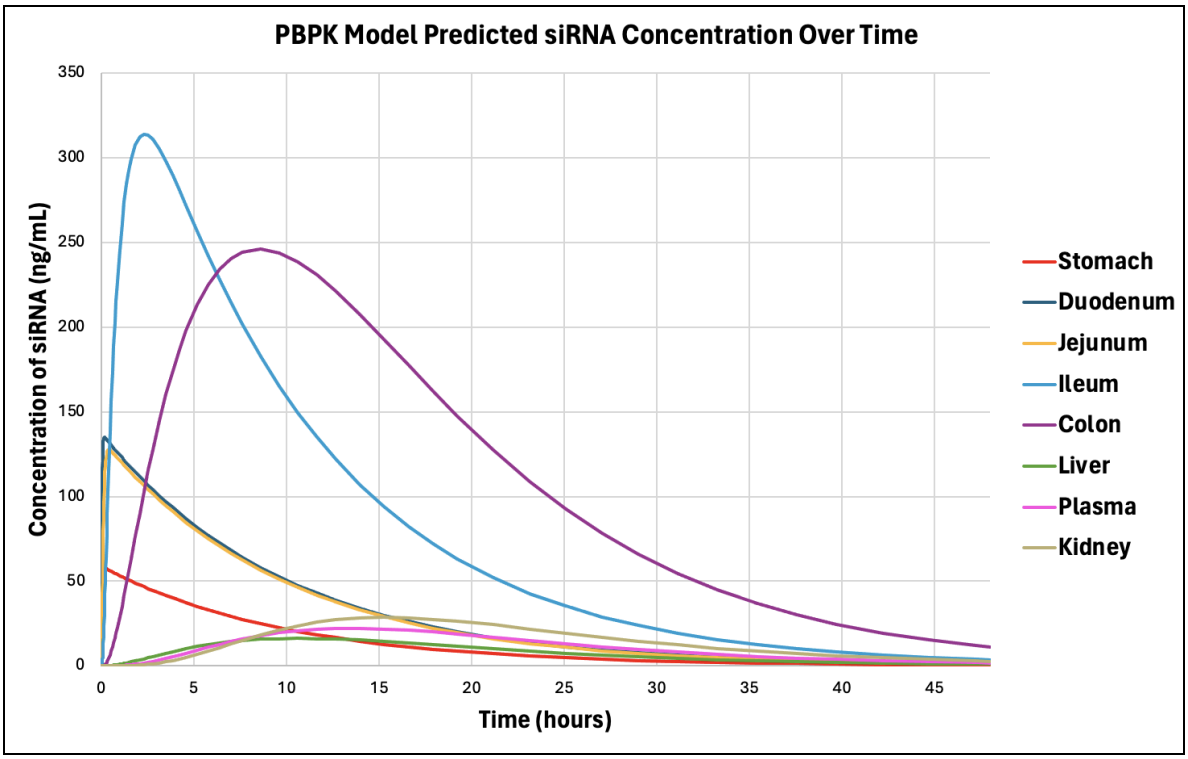

Figure 8 – GI Transfer PBPK Model Simulation Plot. Concentration of siRNA in each compartment simulated over 48 hours.

Table 3 – GI Transfer PBPK Model Simulation Statistics. C_{max} refers to the maximum concentration in the simulated results. AUC refers to the area under the curve for the simulated results.

Compartment	C_{max} (ng/mL)	AUC (ng·h/mL)
Stomach	58.1	583.5
Duodenum	174.6	845.7
Jejunum	123.1	1166.3
Ileum	313.8	3000.2
Colon	264.4	2794.6
Liver	32.6	370.2
Plasma	30.6	291.9
Kidney	23.5	22.3

A comparison of the actual and predicted pharmacokinetic data is shown in Figure 9, where actual refers to the pharmacokinetic data from Attarwala et al., and predicted refers to the simulation results of the GI transfer model. Table 4 quantifies these results by comparing the maximum concentration (C_{max}) and the area under the curve (AUC) for each compartment. The model's predictions for the jejunum, ileum, and colon showed the lowest percent errors for C_{max}, and the predictions for the jejunum, ileum, and liver had the lowest percent errors for AUC, indicating a greater fit to the actual data for these compartments. The kidney compartment exhibited a poor fit, which is likely due to the limited data from the Attarwala et al. study from which only three data points were extracted. Overall, these results suggest that the GI transfer model aligns well with the pharmacokinetic data in several compartments.

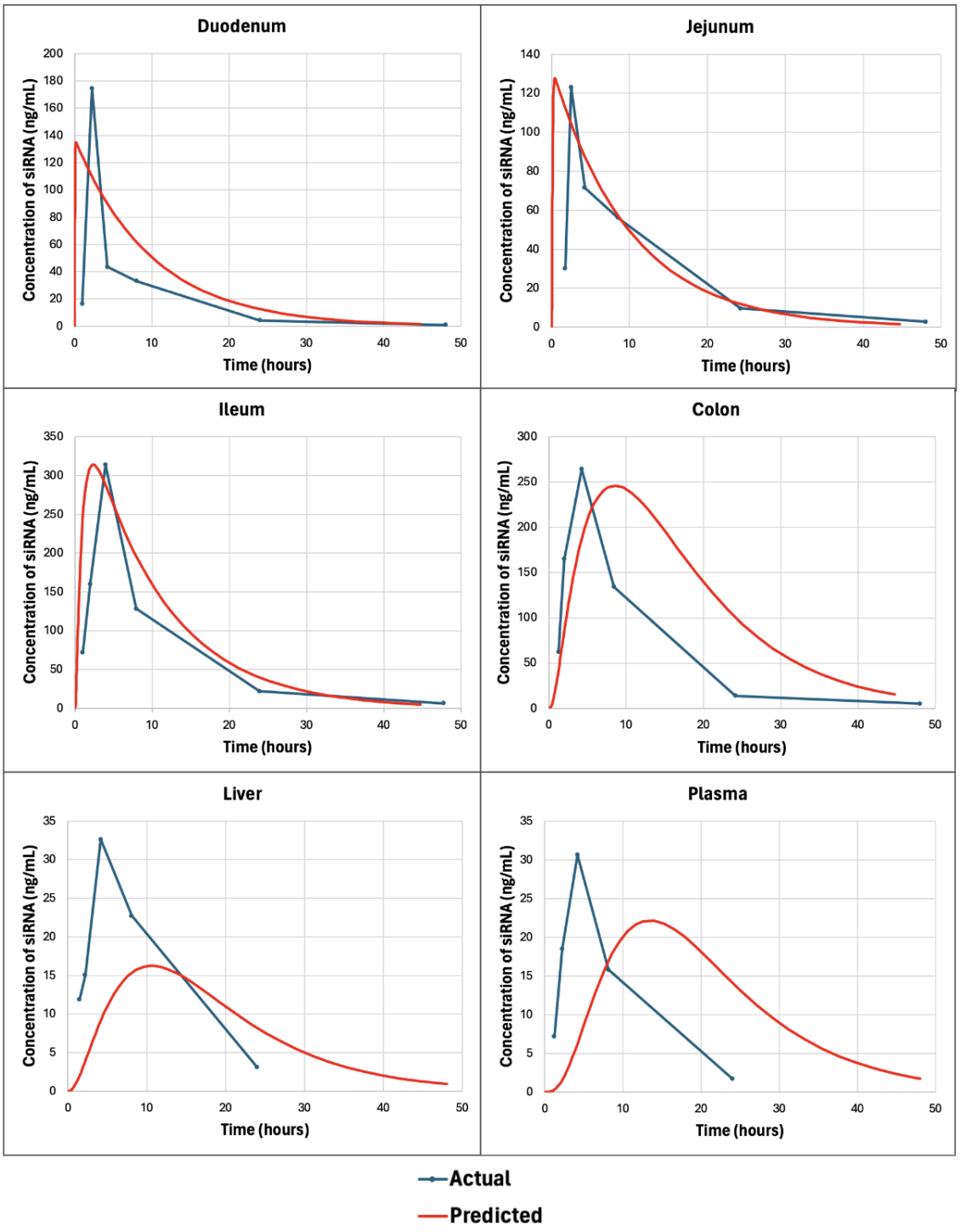

Figure 9 – GI Transfer PBPK Model Simulation Fit. 'Actual' refers to the compartmental pharmacokinetic data from Attarwala et al., and 'Predicted' refers to the results from simulation of the GI Transfer PBPK Model[64].

Table 4 – GI Transfer PBPK Model Rate Sensitivity Analysis Results. C_{max} refers to the maximum concentration in the simulated results.

Compartment	C_{max} (ng/mL) or AUC (ng·h/mL)	Actual	Predicted	Difference	Percent Error (%)
Duodenum	C_{max}	174.6	134.9	39.7	22.7%
	AUC	845.7	1360.4	514.7	60.9%
Jejunum	C_{max}	1166.3	1315	148.7	12.8%
	AUC	123.1	127.6	4.5	3.7%
Ileum	C_{max}	3000.2	3897.6	897.4	29.9%
	AUC	313.7	314.1	0.4	0.1%
Colon	C_{max}	2794.6	5153.2	2358.6	84.4%
	AUC	264.4	246.2	18.2	6.9%
Liver	C_{max}	370.2	360.4	9.8	2.6%
	AUC	32.6	16.2	16.4	50.3%
Plasma	C_{max}	291.9	512.9	221	75.7%
	AUC	30.6	22.1	8.5	27.8%
Kidney	C_{max}	22.3	670	647.7	2904.4%
	AUC	23.5	28.5	5	21.3%

5.2 Gastrointestinal Transfer PBPK Model Sensitivity Analysis

A sensitivity analysis was performed on the GI transfer model to determine the influence of each rate constant on the concentration of siRNA in the ileum. The ileum is one of the most commonly affected regions of the GI tract for patients with IBD, so it is desirable to maximize the concentration of therapeutic siRNA in the ileum[81,82]. Thus, this sensitivity analysis was

performed with the goal of determining which parameters in the model are most impactful on the concentration of siRNA in the ileum. First, a variance-based sensitivity analysis, the Sobol method, was conducted using the MATLAB SimBiology Global Sensitivity Analysis add-on[83]. This analysis tool computes the total-order Sobol index, which quantifies the proportion of the total variance in the output that results from changes in the input parameter, both individually and in conjunction with other parameters[84]. A higher Sobol index indicates that an input parameter has a higher influence on the output result. In this case, the input parameters are the rate constants, and the output result is the concentration of siRNA in the ileum.

The plots of the total-order Sobol indices over time for each rate constant, k_1 - k_{16}, are shown in Figure 10. The plots for k_2 - k_5 and k_{10} - k_{16} reveal that their total-order Sobol indices remain consistently at 0. This suggests that variations in these parameters, either independently or in combination with other parameters, have no discernible effect on the concentration of siRNA reaching the ileum. Importantly, this finding does not definitively rule out the importance of these rate constants under all possible conditions. Rather, it allows these parameters to be deprioritized for future model refinements or experimental validations.

The plots for k_1, k_6, k_7, k_8, and k_9 reveal total-order Sobol indices greater than 0 at one or more points during the simulation period. This indicates that variations in absorption into the stomach (k_1), elimination from the jejunum (k_6), absorption into the ileum (k_7), elimination from the ileum (k_8), and absorption into the colon (k_9), either independently or in combination with other

parameters, significantly impact the concentration of siRNA in the ileum. Thus, this model is highly sensitive to k_1, k_6, k_7, k_8, and k_9.

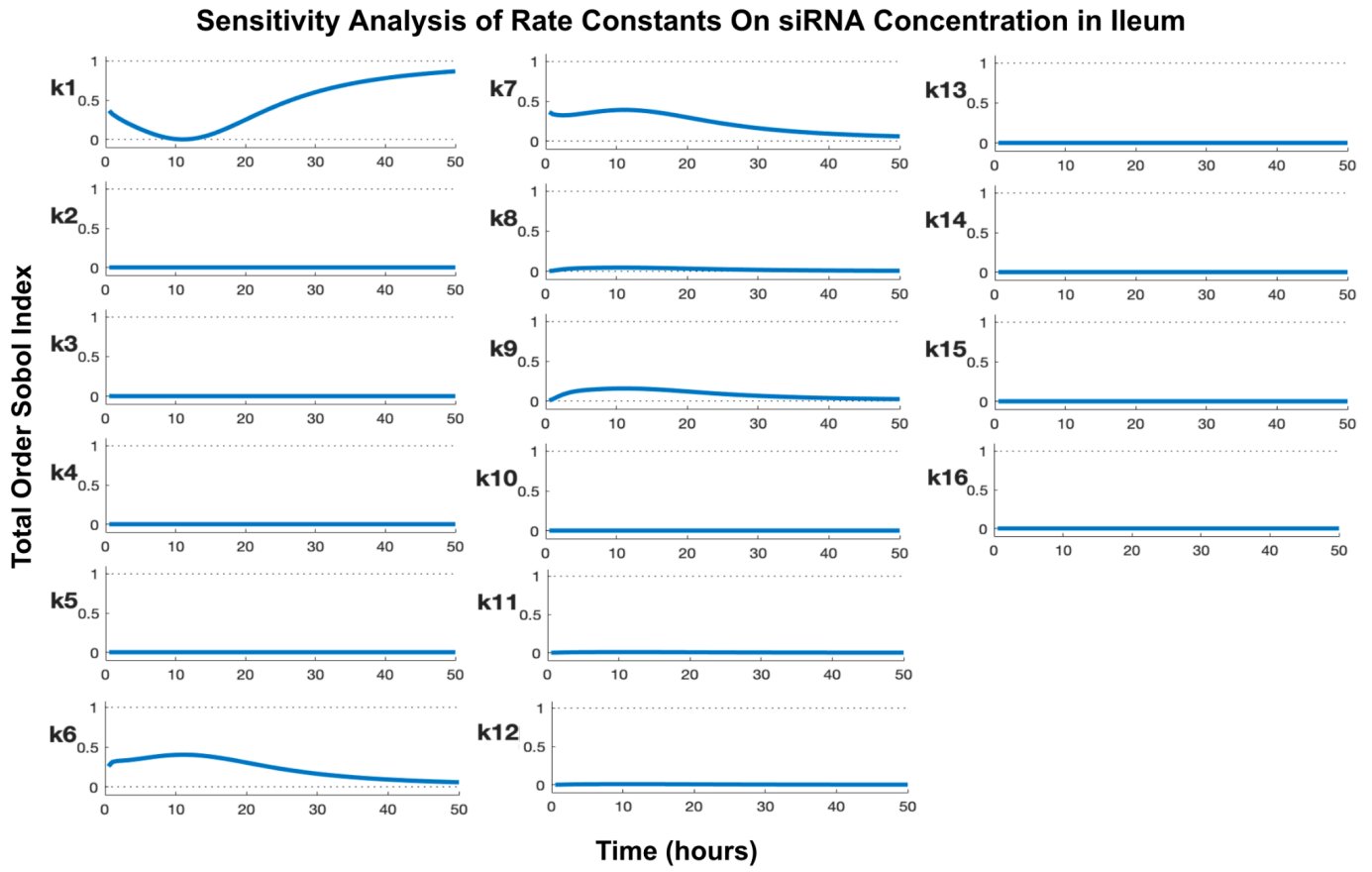

Figure 10 – PBPK Model Sobol Indices over time for variance in ileum concentration of siRNA. Indices were calculated using the MATLAB SimBiology Global Sensitivity Analysis add-on.

Given that the model is sensitive to k_1, k_6, k_7, k_8 and k_9, a second sensitivity analysis was conducted to determine which of these rate constants has the greatest impact. To do this, the GI transfer PBPK model was simulated multiple times, each with one rate constant, k_1, k_6, k_7, k_8 and k_9, decreased or increased by 50% from its original value. For example, with k_1 originally at 0.1 hr^{-1}, simulations were run at adjusted values of 0.05 hr^{-1} and 0.15 hr^{-1}. Similarly, k_6, which

was originally 13 hr^{-1}, was simulated at 6.5 and 19.5 hr^{-1}; k_7 and k_8, which were originally 0.3676 hr^{-1}, were simulated at 0.1838 and 0.5514 hr^{-1}; and k_9, originally 0.6917 hr^{-1}, was simulated at 0.34585 and 1.03755 hr^{-1}.

The plots of the concentration of siRNA in the ileum over time for each set of simulations with varied rate constants is shown in Figure 11. Each subplot includes three simulations with a given rate constant at its original value, decreased by 50%, and increased by 50%. The results show the effect each constant has on the concentration of siRNA in the ileum over time, and the resulting maximum concentrations (C_{max}) of each simulation are detailed in Table 5. As revealed by the C_{max} results, a given variation in k_1, k_6 and k_7 has a greater impact on C_{max} than the same variation in k_8 and k_9. This suggests that the GI transfer PBPK model is most sensitive to variations in absorption into the stomach (k_1), elimination from the jejunum (k_6), and absorption into the ileum (k_7) and that these constants play a pivotal role in the concentration of siRNA that is delivered to the ileum. Consequently, these findings highlight areas where parameter estimation refinement and experimental validation are crucial for improving the model's predictive accuracy. Furthermore, future work in optimizing siRNA delivery can prioritize focus on siRNA absorption into the stomach (k_1), elimination from the jejunum (k_6), and absorption into the ileum (k_7) .

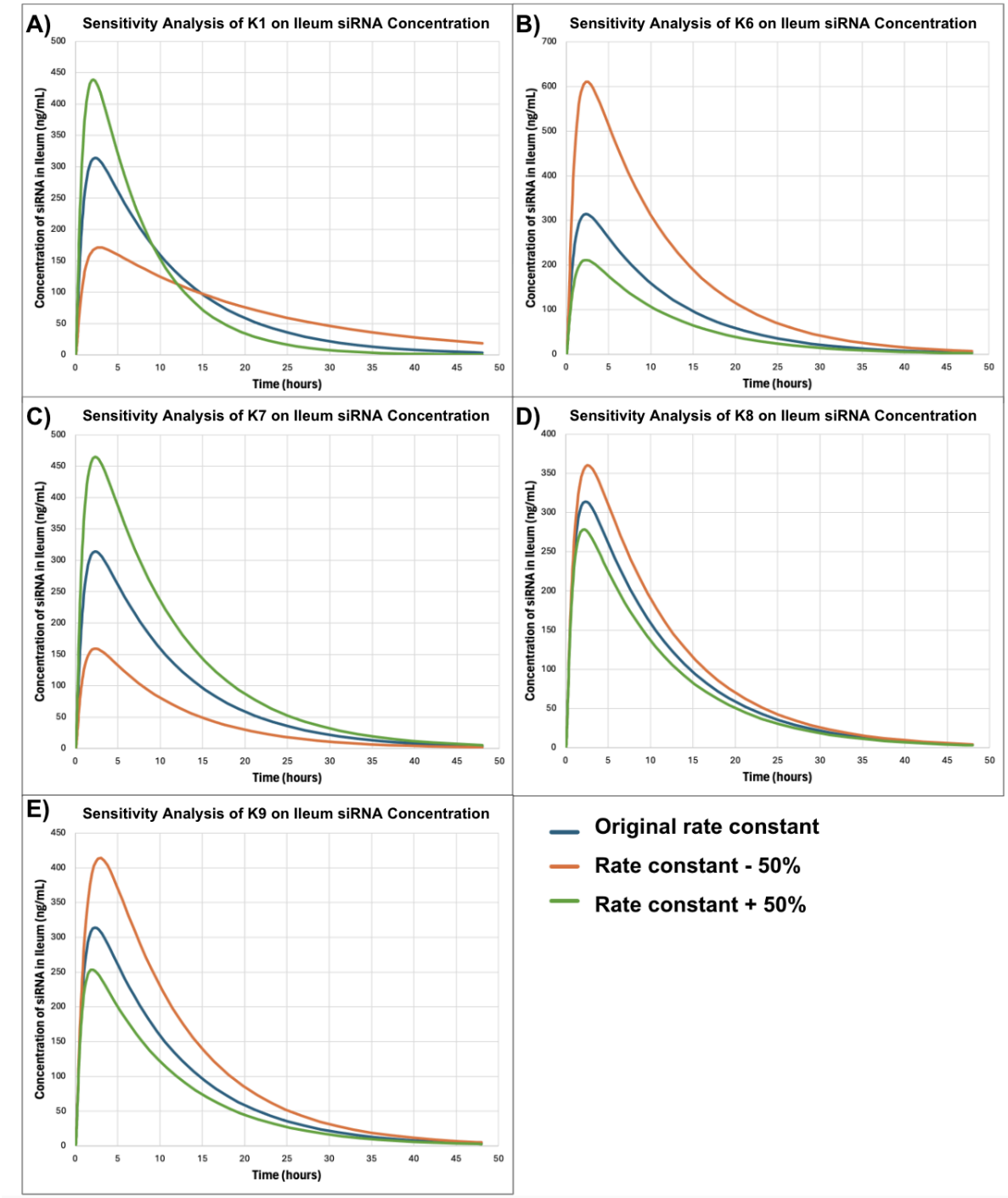

Figure 11 – GI Transfer PBPK Model Sensitivity Analysis given variations in **A)** k_1 **B)** k_6 **C)** k_7 **D)** k_8 **E)** k_9. The simulation using the original value of the rate constant is blue, the simulation using the rate constant decreased by 50% is orange, and the simulation using the rate constant increased by 50% is green.

Table 5 – GI Transfer PBPK Model Rate Sensitivity Analysis Results. C_{max} refers to the maximum concentration in the simulated results.

Parameter	Description	Difference in C_{max} with rate constant decreased by 50% (ng/mL)	Difference in C_{max} with rate constant increased by 50% (ng/mL)
k_1	$k_{absorption,\ stomach}$	-142.8	+124.9
k_6	$k_{elimination,\ jejunum}$	+296.5	-102.9
k_7	$k_{absorption,\ ileum}$	-314.2	+150.7
k_8	$k_{elimination,\ ileum}$	+46.1	-35.6
k_9	$k_{absorption,\ colon}$	+99.8	-60.6

While the focus of this analysis was on the ileum, reflecting the priorities of an IBD treatment strategy, the same model can be used to analyze other parameters and achieve different goals. For instance, a plasma sensitivity analysis can be useful to study how siRNA circulates through the bloodstream in a future application where systemic distribution is desirable. This might be relevant if oral administration of siRNA is used to treat conditions beyond IBD or if there is a need for a systemic therapeutic effect. By assessing the rate constants that influence plasma concentrations, a broader understanding of siRNA dynamics can be achieved, allowing us to understand how to prioritize siRNA delivery into circulation for future studies.

Thus, a sensitivity analysis was performed on the GI transfer PBPK model to determine the influence of each rate constant on the concentration of siRNA in the plasma. As in the previous

sensitivity analysis for the ileum, a variance-based sensitivity analysis, the Sobol method, was conducted using the MATLAB SimBiology Global Sensitivity Analysis add-on[83]. This analysis tool computes the total-order Sobol index, where a higher Sobol index indicates that an input parameter has a higher influence on the output result. In this case, the input parameters are the rate constants, and the output result is the concentration of siRNA in the plasma.

The plots of the total-order Sobol indices over time for each rate constant, k_1 - k_{16}, are shown in Figure 12. The plots for k_2 - k_5 and k_9, k_{10}, k_{12}, k_{14}, and k_{16} reveal that their total-order Sobol indices remain consistently at 0. This suggests that variations in these parameters, either independently or in combination with other parameters, have no discernible effect on the concentration of siRNA reaching the plasma.

The plots for k_1, k_6, k_7, k_8, k_{11}, k_{13}, and k_{15} reveal total-order Sobol indices greater than 0 at one or more points during the simulation period. This indicates that variations in absorption into the stomach (k_1), elimination from the jejunum (k_6), absorption into the ileum (k_7), elimination from the ileum (k_8), absorption into the liver (k_{11}), absorption into the plasma (k_{13}), and absorption into the kidney (k_{15}), either independently or in combination with other parameters, impact the concentration of siRNA in the plasma.

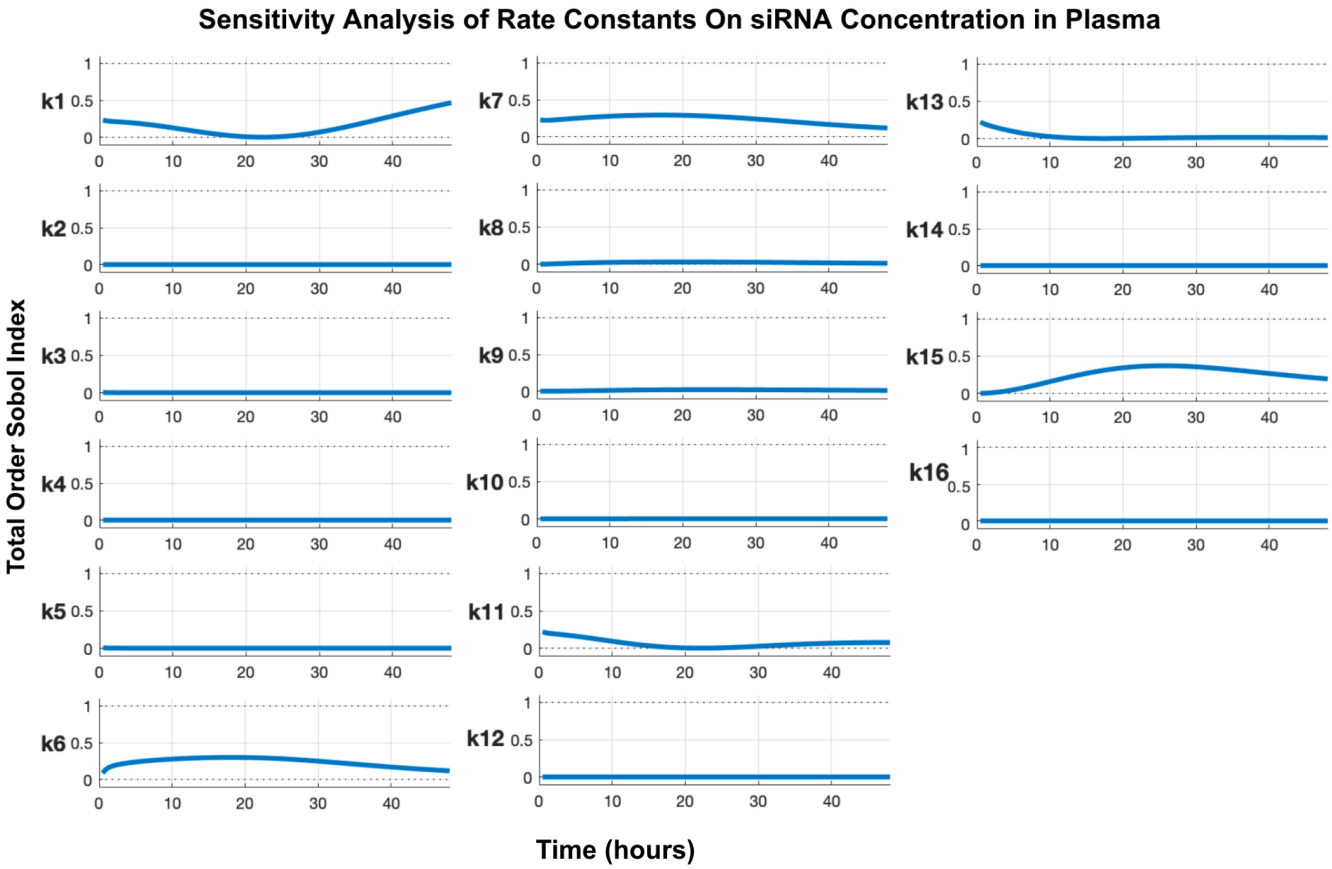

Figure 12 – PBPK Model Sobol Indices over time for variance in plasma concentration of siRNA. Indices were calculated using the MATLAB SimBiology Global Sensitivity Analysis add-on.

By conducting this analysis, the GI transfer PBPK model provides a useful tool for understanding and optimizing siRNA delivery into plasma circulation. This capability can be valuable for future studies or applications where delivery into circulation is a priority. It highlights the versatility of the model and suggests that similar analyses can be used in future research to explore different delivery pathways for siRNA therapeutic strategies.

5.3 Cell PBPK Model

A cell PBPK model was proposed to describe the pharmacokinetics of siRNA once it reaches the cell. Once in the target tissue, it must be endosomally uptaken into the cell, released into the cytoplasm, and bound to the RISC complex. Once bound to RISC, it can cleave the target mRNA and silence the gene. The compartmental model proposed for this is shown in Figure 10, which depicts the overall schematic in Figure 10A and the model as it appears in MATLAB SimBiology in Figure 10B. The rate constants used to define the model are listed in Table 3. The model includes three compartments. It begins with the endosome compartment, where the initial dose is delivered in the model to represent the amount of siRNA that reaches the target tissue. In this case, the target tissue is the ileum. In the endosome, the siRNA is either degraded or released into the second compartment, the cytoplasm. In the cytoplasm, the siRNA is either degraded or loaded onto the third compartment, the RISC complex. The RISC-loaded siRNA is either degraded or unloaded from the RISC complex.

Three ordinary differential equations describe this PBPK model:

$$\frac{dC_{Endosome}}{dt} = k_1 * C_{Dose} - k_2 * C_{Endosome} - k_3 * C_{Endosome}$$

$$\frac{dC_{Cytoplasm}}{dt} = k_3 * C_{Endosome} - k_4 * C_{Cytoplasm} - k_5 * C_{Cytoplasm} + k_6 * C_{RISC}$$

$$\frac{dC_{RISC}}{dt} = k_5 * C_{Cytoplasm} - k_6 * C_{RISC} - k_7 * C_{RISC}$$

where, k_1 = Endosomal uptake of ileum siRNA, k_2 = Degradation of endosomal siRNA, k_3 = Endosomal escape, k_4 = Degradation of free cytoplasmic siRNA, k_5 = Association of siRNA to the RISC complex, k_6 = Dissociation of siRNA from the RISC complex, and k_7 = Degradation of RISC-loaded siRNA.

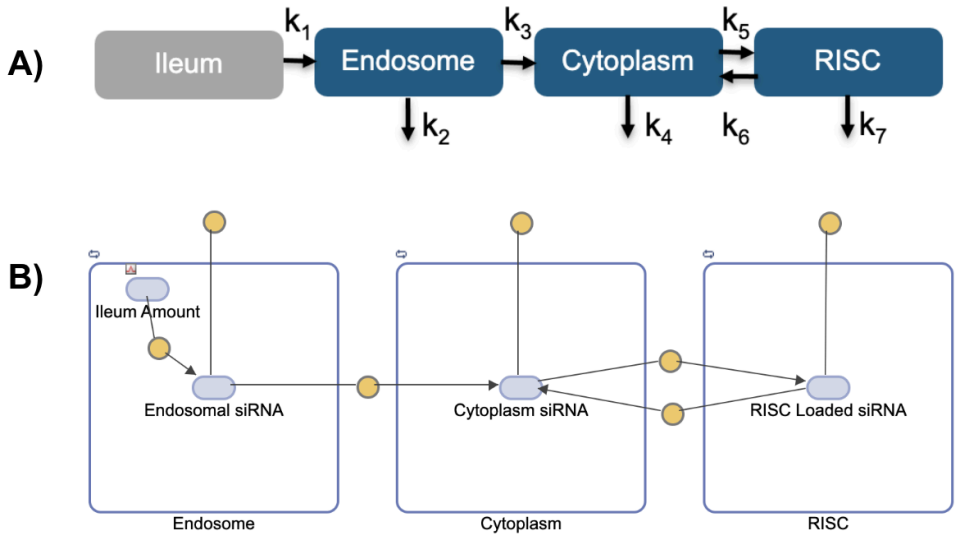

Figure 13 – Cell PBPK Model Schematics. The model includes 3 compartments: Endosome, Cytoplasm, and RISC. **A)** General schematic. **B)** Schematic built in MATLAB SimBiology Model Builder tool. Each compartment includes species blocks (blue) to represent the amount of siRNA and reaction blocks (yellow) to define the rate of movement of siRNA from one compartment to another. The initial amount of 'Endosomal siRNA' is defined by the amount dosed into the 'Ileum amount' species.

Table 6 – Cell PBPK Model Rate Constants. All rate constants were acquired from literature[78,79].

Parameter	**Description**	**Rate (hr^{-1})**
k_1	Endosomal uptake of ileum siRNA	1
k_2	Degradation of endosomal siRNA	0.012
k_3	Endosomal escape	0.06
k_4	Degradation of free cytoplasmic siRNA	0.1
k_5	Association of siRNA to the RISC complex	0.00023
k_6	Dissociation of siRNA from the RISC complex	0.000001
k_7	Degradation of RISC-loaded siRNA	0.005

The goal of this model was to calculate the amount of RISC-loaded siRNA over time. Because only RISC-loaded siRNA can cleave and silence the target mRNA, measuring the amount of RISC-loaded siRNA can indicate the gene-silencing ability of siRNA and improve understanding of how to maximize its therapeutic effect. This model was simulated with a 1000 ng dose to the Endosome compartment. This represents that 1000 ng of an orally administered dose of siRNA was delivered to this cell in the target tissue, the ileum. The results from this simulation are in Figure 11, which plots the amount of RISC-loaded siRNA over time. The maximum concentration of RISC-loaded siRNA in this simulation was 1.532 nanograms at 56.6 hours.

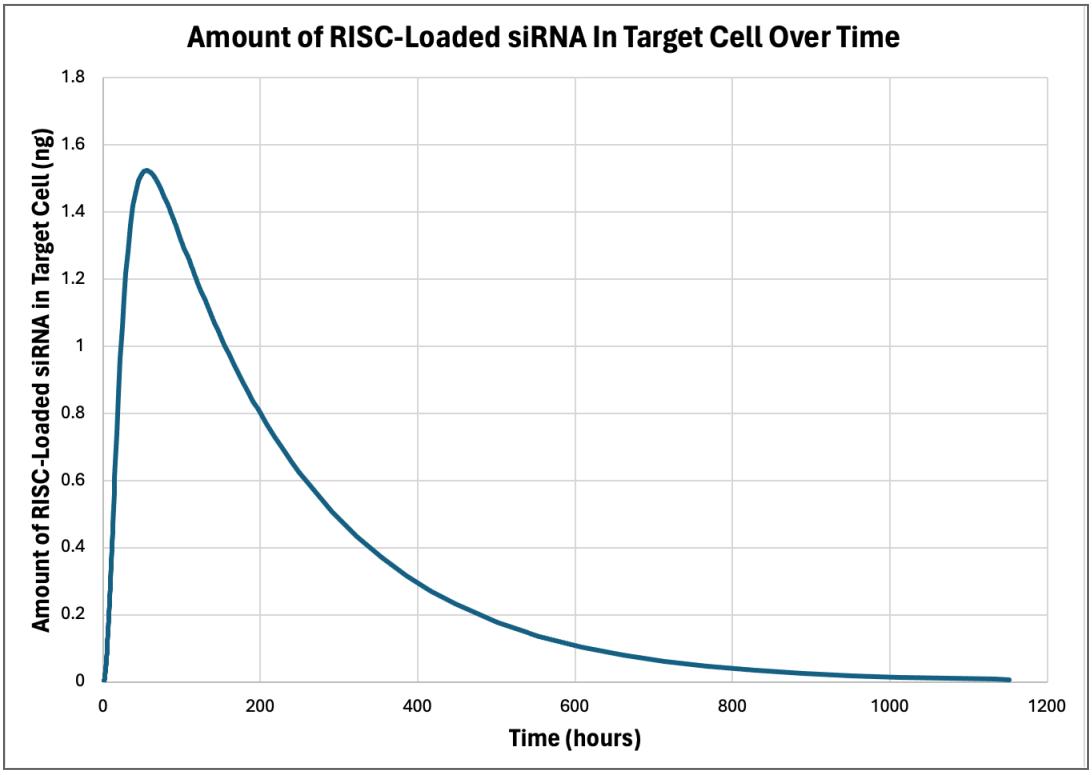

Figure 14 – Cell PBPK Model Simulation Plot. The model was simulated over 1152 hours given a 1000 ng instant bolus dose at time 0. The simulation result shows the amount of RISC-Loaded siRNA over time.

5.4 Cell PBPK Model Sensitivity Analysis

A sensitivity analysis was performed on the cell PBPK model to determine the influence of each rate constant on the amount of RISC-loaded siRNA. The goal of this analysis was to determine which parameters within the cell are most impactful on gene silencing, with the amount of RISC-loaded siRNA acting as a quantitative proxy for gene silencing abilities. As in the previous sensitivity analysis on the GI transfer model, a variance-based sensitivity analysis, the Sobol method, was conducted using the MATLAB SimBiology Global Sensitivity Analysis add-on[83]. This analysis tool computes the total-order Sobol index, and a higher Sobol index indicates that an input parameter has a higher influence on the output result. In this case, the input parameters are the rate constants, and the output result is the amount of RISC-loaded siRNA.

The plots of the total-order Sobol indices over time for each rate constant, k_1 - k_7, are shown in Figure 12. The plots for k_1, k_2, and k_6 reveal that their total-order Sobol indices remain consistently at 0. This suggests that variations in endosomal uptake of ileum siRNA (k_1), degradation of endosomal siRNA (k_2), and dissociation of siRNA from RISC (k_6), either independently or in combination with other parameters, have no discernable impact on the amount of RISC-loaded siRNA in this model. Importantly, this finding does not definitively rule out the importance of these three rate constants under all possible conditions. Rather, it allows these parameters to be deprioritized for future model refinements or experimental validations.

The plots for k_3, k_4, k_5 and k_7 reveal total-order Sobol indices greater than 0 at one or more points during the simulation period. This indicates that variations in endosomal escape of siRNA (k_3), degradation of free cytoplasmic siRNA (k_4), association of siRNA to RISC (k_5), and degradation of RISC-loaded siRNA (k_7), either independently or in combination with other parameters, significantly impact the amount of RISC-loaded siRNA in this model.

Thus, this model is highly sensitive to k_3, k_4, k_5 and k_7 for varying durations during the simulation period. Endosomal escape (k_3) has a high impact index in the first 50 hours of simulation and has a negligible impact after 50 hours, likely because all of the initial dose has been transported out of the endosome compartment by that point. Degradation of free cytoplasmic siRNA (k_4) and association of siRNA to RISC (k_5) have a high impact index throughout the majority of the simulation and decrease in impact near the end, when the majority of siRNA is likely degraded or loaded onto RISC. Degradation of RISC-loaded siRNA (k_7) has a negligible impact index in the first 100 hours, likely because siRNA has not yet been transported into the RISC compartment, and has increasing impact over time after 100 hours.

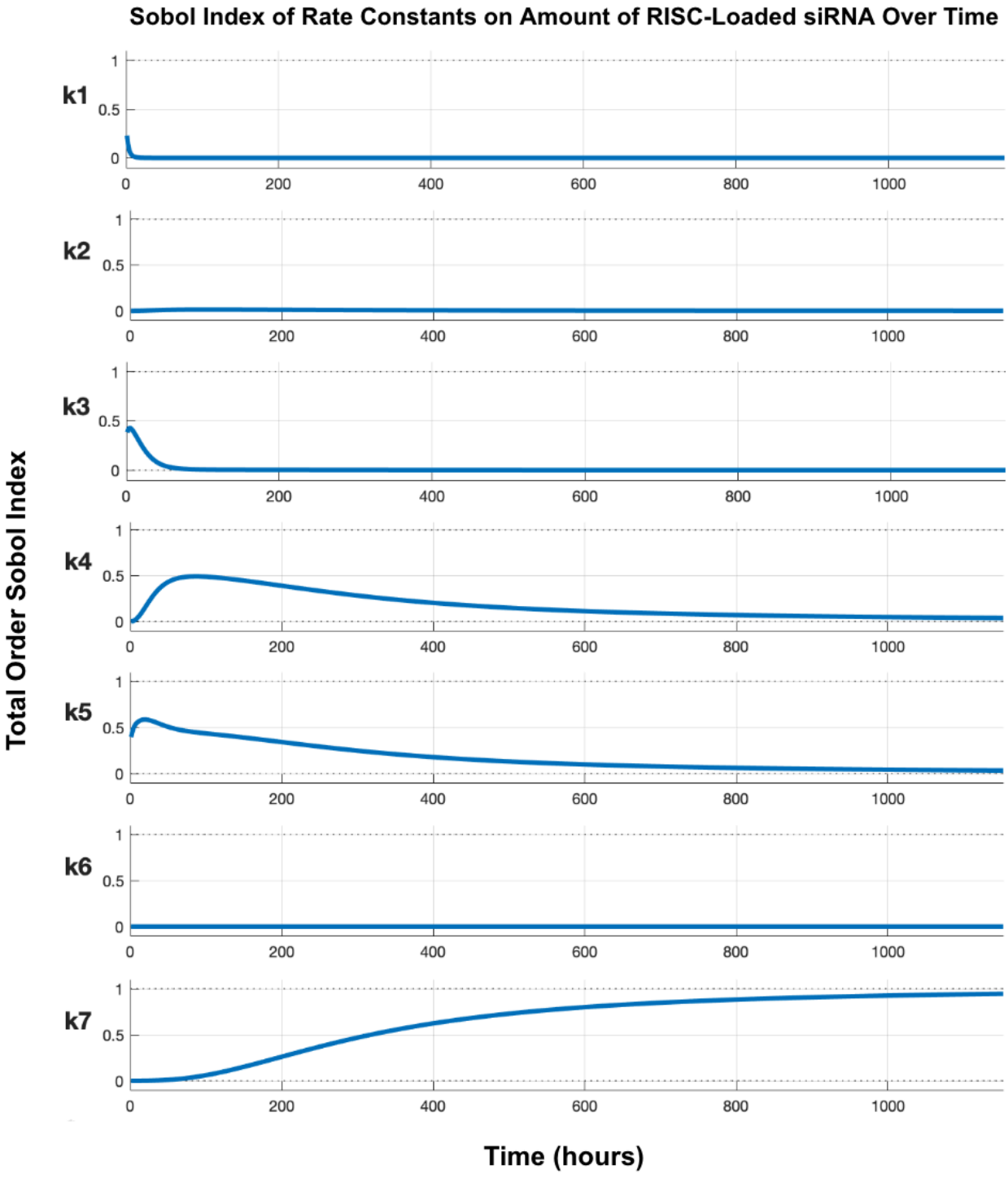

Figure 15 – Cell PBPK Model Sobol Indices over time. Indices were calculated using the MATLAB SimBiology Global Sensitivity Analysis add-on.

Given that the model is sensitive to k_3, k_4, k_5 and k_7, a second sensitivity analysis was conducted to determine which of these rate constants has the greatest impact. To do this, the cell PBPK model was simulated multiple times, each with one rate constant, k_3, k_4, k_5 or k_7, decreased or increased by 50% from its original value. For example, with k_3 originally at 0.06 hr^{-1}, simulations were run at adjusted values of 0.03 hr^{-1} and 0.09 hr^{-1}. Similarly, k_4, which was originally 0.1 hr^{-1}, was simulated at 0.05 and 0.15 hr^{-1}; k_5, which was originally 0.00023 hr^{-1}, was simulated at 0.000115 and 0.000345 hr^{-1}; and k_7, originally 0.005 hr^{-1}, was simulated at 0.0025 and 0.0075 hr^{-1}.

The plots of the amount of RISC-loaded siRNA over time for each set of simulations with varied rate constants is shown in Figure 13. Each subplot includes three simulations with a given rate constant at its original value, decreased by 50%, and increased by 50%. The results show the effect each constant has on the amount of RISC-loaded siRNA over time, and the resulting maximum concentrations (C_{max}) of each simulation are detailed in Table 3. As revealed by the C_{max} results, a given variation in k_4 and k_5 has a greater impact on C_{max} than the same variation in k_3 and k_7. This suggests that the cell PBPK model is most sensitive to variations in the absorption into the stomach (k_4) and association of siRNA to RISC (k_5) and that these constants play a pivotal role in the amount of siRNA that gets loaded onto the RISC complex. Consequently, these findings highlight areas where parameter estimation refinement and experimental validation are crucial for improving the model's predictive accuracy. Furthermore, future work in optimizing siRNA delivery can prioritize focus on the degradation of free siRNA

(k_4) and the association of siRNA to the RISC complex (k_5).

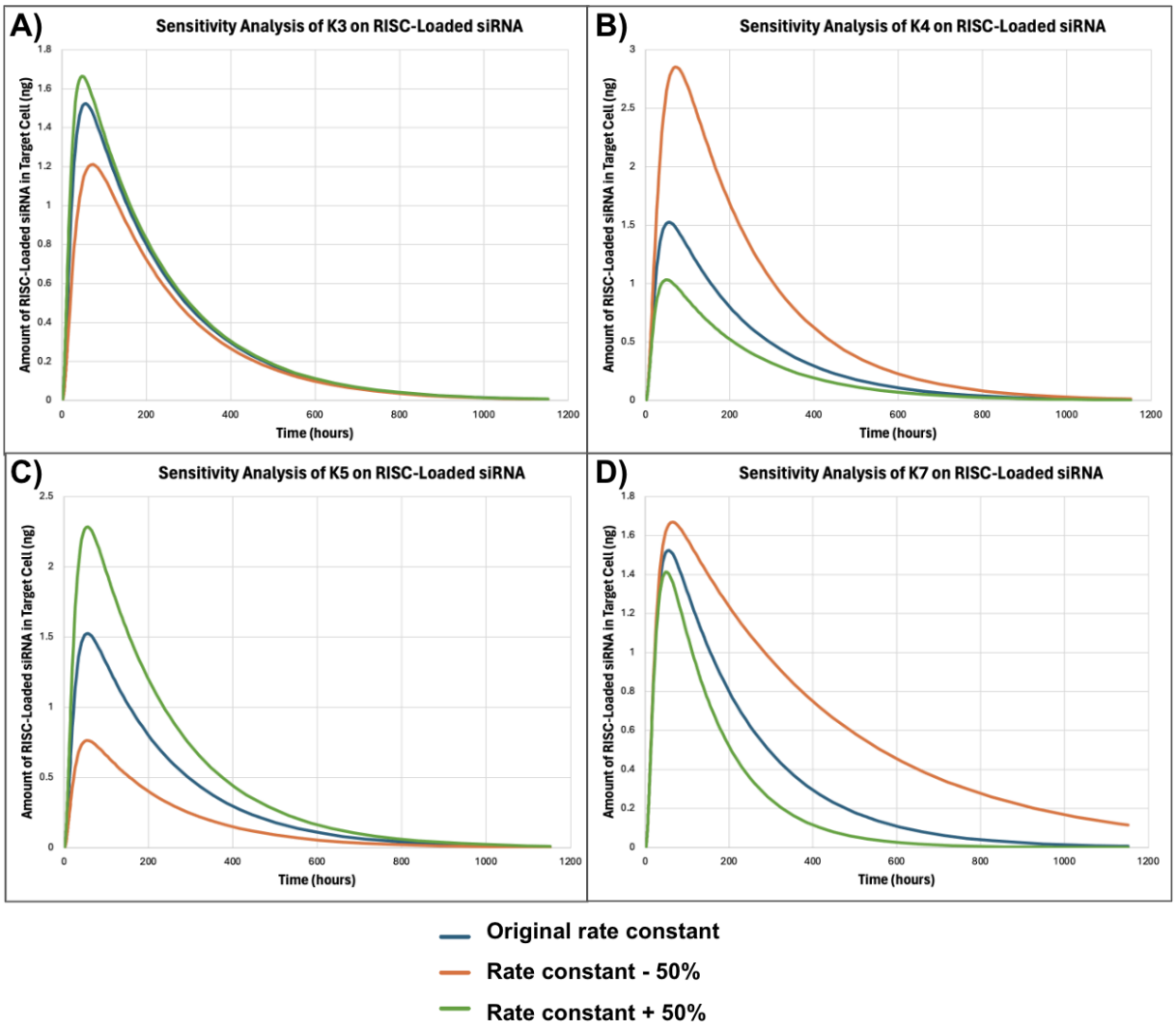

Figure 16 – Cell PBPK Model Sensitivity Analysis given variations in **A)** k_3 **B)** k_4 **C)** k_5 **D)** k_7. The simulation using the original value of rate constant is blue, the simulation using the rate constant decreased by 50% is orange, and the simulation using the rate constant increased by 50% is green.

Table 7 – Cell PBPK Model Rate Sensitivity Analysis Results. C_{max} refers to the maximum concentration in the simulated results.

Parameter	**Description**	**Difference in C_{max} with rate constant decreased by 50% (ng/mL)**	**Difference in C_{max} with rate constant increased by 50% (ng/mL)**
k_3	Endosomal escape	-0.31	+0.14
k_4	Degradation of free cytoplasmic siRNA	+1.33	-0.49
k_5	Association of siRNA to the RISC complex	-0.76	+0.76
k_7	Degradation of RISC-loaded siRNA	+0.15	-0.11

CHAPTER 6

CONCLUSIONS AND RECOMMENDATIONS

This thesis aimed to investigate the pharmacokinetics of orally administered small interfering RNA (siRNA) for the treatment of Inflammatory Bowel Disease (IBD). To achieve this, a comprehensive literature review was conducted to find pharmacokinetic data that could inform the construction of two distinct physiologically based pharmacokinetic (PBPK) models: one for gastrointestinal (GI) transfer and the other for cellular dynamics.

The first model, the GI transfer PBPK model, examined the pharmacokinetics of orally administered siRNA in eight compartments, from the stomach to the kidneys, with special attention on the ileum and colon — key regions for IBD treatment. Parameters such as compartment volumes, absorption rate constants, and elimination rate constants were derived from literature, data fitting, and parameter estimation. Sensitivity analyses indicated that absorption into the stomach, elimination from the jejunum, and absorption into the ileum are critical to the siRNA concentration in the ileum. This suggests that optimizing these rate constants could improve therapeutic outcomes for IBD. The GI transfer model provided valuable insights into the absorption, distribution, and elimination of siRNA, forming a foundational tool for exploring the pharmacokinetics of oral siRNA therapies.

The second model, the cell PBPK model, focused on the intracellular journey of siRNA once it reaches target cells in the ileum. This model described endosomal uptake, cytoplasmic release, and binding to the RNA-induced silencing complex (RISC), key steps in the gene-silencing pathway. Sensitivity analyses on this model revealed that the rate constants for degradation of

free cytoplasmic siRNA and association to RISC significantly impact the gene-silencing potential of siRNA. This model's insights are crucial for understanding siRNA's cellular dynamics, providing a roadmap for optimizing therapeutic strategies at the cellular level.

Furthermore, the versatility of the PBPK models was demonstrated through a plasma sensitivity analysis, indicating the models' potential for exploring different therapeutic strategies beyond IBD, where systemic distribution may be essential. This flexibility suggests that the models can be adapted to study various diseases and applications of siRNA-based treatments.

In light of these findings, several recommendations emerge. To refine the PBPK models, additional pharmacokinetic data and experimental validation are needed to improve the accuracy of the rate constants. This involves more comprehensive studies that measure siRNA pharmacokinetics under various conditions, including oral administration, intravenous administration, and with various nanoparticle encapsulations. For the GI transfer model, focusing on the key rate constants that affect absorption and elimination can help optimize siRNA delivery to target compartments. For the cell model, optimizing the rate constants associated with endosomal escape, cytoplasmic degradation, and RISC complex dynamics can enhance siRNA's therapeutic efficacy.

These conclusions and recommendations aim to guide future research on PBPK modeling and siRNA therapeutics, emphasizing the importance of refining models, conducting experimental validation, and exploring broader applications for improving IBD treatment and advancing the field of siRNA-based therapy.

REFERENCES

(1) *People with IBD Have More Chronic Diseases | CDC*. https://www.cdc.gov/ibd/features/IBD-more-chronic-diseases.html (accessed 2023-11-27).

(2) Borowitz, S. M. The Epidemiology of Inflammatory Bowel Disease: Clues to Pathogenesis? *Front. Pediatr.* 2023, *10*, 1103713. https://doi.org/10.3389/fped.2022.1103713.

(3) Panaccione, R. Mechanisms of Inflammatory Bowel Disease. *Gastroenterol. Hepatol.* 2013, *9* (8), 529–532.

(4) Jairath, V.; Feagan, B. G. Global Burden of Inflammatory Bowel Disease. *Lancet Gastroenterol. Hepatol.* 2020, *5* (1), 2–3. https://doi.org/10.1016/S2468-1253(19)30358-9.

(5) Ellinghaus, D.; Bethune, J.; Petersen, B.-S.; Franke, A. The Genetics of Crohn's Disease and Ulcerative Colitis – Status Quo and Beyond. *Scand. J. Gastroenterol.* 2015, *50* (1), 13–23. https://doi.org/10.3109/00365521.2014.990507.

(6) Loddo, I.; Romano, C. Inflammatory Bowel Disease: Genetics, Epigenetics, and Pathogenesis. *Front. Immunol.* 2015, *6*.

(7) Soon, I. S.; Molodecky, N. A.; Rabi, D. M.; Ghali, W. A.; Barkema, H. W.; Kaplan, G. G. The Relationship between Urban Environment and the Inflammatory Bowel Diseases: A Systematic Review and Meta-Analysis. *BMC Gastroenterol.* 2012, *12* (1), 51. https://doi.org/10.1186/1471-230X-12-51.

(8) Ng, S. C.; Bernstein, C. N.; Vatn, M. H.; Lakatos, P. L.; Loftus, E. V.; Tysk, C.; O'Morain, C.; Moum, B.; Colombel, J.-F. Geographical Variability and Environmental Risk Factors in Inflammatory Bowel Disease. *Gut* 2013, *62* (4), 630. https://doi.org/10.1136/gutjnl-2012-303661.

(9) Khalili, H.; Chan, S. S. M.; Lochhead, P.; Ananthakrishnan, A. N.; Hart, A. R.; Chan, A. T. The Role of Diet in the Aetiopathogenesis of Inflammatory Bowel Disease. *Nat. Rev. Gastroenterol. Hepatol.* 2018, *15* (9), 525–535. https://doi.org/10.1038/s41575-018-0022-9.

(10) Piovani, D.; Danese, S.; Peyrin-Biroulet, L.; Bonovas, S. Environmental, Nutritional, and Socioeconomic Determinants of IBD Incidence: A Global Ecological Study. *J. Crohns Colitis* 2020, *14* (3), 323–331. https://doi.org/10.1093/ecco-jcc/jjz150.

(11) Ananthakrishnan, A. N.; Bernstein, C. N.; Iliopoulos, D.; Macpherson, A.; Neurath, M. F.; Ali, R. A. R.; Vavricka, S. R.; Fiocchi, C. Environmental Triggers in IBD: A Review of Progress and Evidence. *Nat. Rev. Gastroenterol. Hepatol.* 2018, *15* (1), 39–49. https://doi.org/10.1038/nrgastro.2017.136.

(12) Lee, S. H.; Kwon, J. eun; Cho, M.-L. Immunological Pathogenesis of Inflammatory Bowel Disease. *Intest. Res.* 2018, *16* (1), 26–42. https://doi.org/10.5217/ir.2018.16.1.26.

(13) Guan, Q. A Comprehensive Review and Update on the Pathogenesis of Inflammatory Bowel Disease. *J. Immunol. Res.* 2019, *2019*, e7247238. https://doi.org/10.1155/2019/7247238.

(14) Cai, Z.; Wang, S.; Li, J. Treatment of Inflammatory Bowel Disease: A Comprehensive Review. *Front. Med.* 2021, *8*.

(15) Chapman, T. P.; Frias Gomes, C.; Louis, E.; Colombel, J.-F.; Satsangi, J. Review Article: Withdrawal of 5-Aminosalicylates in Inflammatory Bowel Disease. *Aliment. Pharmacol. Ther.* 2020, *52* (1), 73–84. https://doi.org/10.1111/apt.15771.

(16) Park, J.; Cheon, J. H. Updates on Conventional Therapies for Inflammatory Bowel Diseases: 5-Aminosalicylates, Corticosteroids, Immunomodulators, and Anti-TNF-α. *Korean J. Intern. Med.* 2022, *37* (5), 895–905. https://doi.org/10.3904/kjim.2022.132.

(17) Egan, L. J.; Mays, D. C.; Huntoon, C. J.; Bell, M. P.; Pike, M. G.; Sandborn, W. J.; Lipsky, J. J.; McKean, D. J. Inhibition of Interleukin-1-Stimulated NF-kappaB RelA/P65 Phosphorylation by Mesalamine Is Accompanied by Decreased Transcriptional Activity. *J. Biol. Chem.* 1999, *274* (37), 26448–26453. https://doi.org/10.1074/jbc.274.37.26448.

(18) Sandborn, W. J.; Hanauer, S. B. Systematic Review: The Pharmacokinetic Profiles of Oral Mesalazine Formulations and Mesalazine pro-Drugs Used in the Management of Ulcerative Colitis. *Aliment. Pharmacol. Ther.* 2003, *17* (1), 29–42. https://doi.org/10.1046/j.1365-2036.2003.01408.x.

(19) Layer, P. H.; Goebell, H.; Keller, J.; Dignass, A.; Klotz, U. Delivery and Fate of Oral Mesalamine Microgranules within the Human Small Intestine. *Gastroenterology* 1995, *108* (5), 1427–1433. https://doi.org/10.1016/0016-5085(95)90691-6.

(20) Gisbert, J. P.; González-Lama, Y.; Maté, J. 5-Aminosalicylates and Renal Function in Inflammatory Bowel Disease: A Systematic Review. *Inflamm. Bowel Dis.* 2007, *13* (5), 629–638. https://doi.org/10.1002/ibd.20099.

(21) Irving, P. M.; Gearry, R. B.; Sparrow, M. P.; Gibson, P. R. Review Article: Appropriate Use of Corticosteroids in Crohn's Disease. *Aliment. Pharmacol. Ther.* 2007, *26* (3), 313–329. https://doi.org/10.1111/j.1365-2036.2007.03379.x.

(22) Ford, A. C.; Bernstein, C. N.; Khan, K. J.; Abreu, M. T.; Marshall, J. K.; Talley, N. J.; Moayyedi, P. Glucocorticosteroid Therapy in Inflammatory Bowel Disease: Systematic Review and Meta-Analysis. *Off. J. Am. Coll. Gastroenterol. ACG* 2011, *106* (4), 590. https://doi.org/10.1038/ajg.2011.70.

(23) Neurath, M. Thiopurines in IBD. *Gastroenterol. Hepatol.* 2010, *6* (7), 435–436.

(24) Kapur, S.; Hanauer, S. B. The Evolving Role of Thiopurines in Inflammatory Bowel

Disease. *Curr. Treat. Options Gastroenterol.* 2019, *17* (3), 420–433. https://doi.org/10.1007/s11938-019-00244-3.

(25) Singh, A.; Mahajan, R.; Kedia, S.; Dutta, A. K.; Anand, A.; Bernstein, C. N.; Desai, D.; Pai, C. G.; Makharia, G.; Tevethia, H. V.; Mak, J. W.; Kaur, K.; Peddi, K.; Ranjan, M. K.; Arkkila, P.; Kochhar, R.; Banerjee, R.; Sinha, S. K.; Ng, S. C.; Hanauer, S.; Verma, S.; Dutta, U.; Midha, V.; Mehta, V.; Ahuja, V.; Sood, A. Use of Thiopurines in Inflammatory Bowel Disease: An Update. *Intest. Res.* 2021, *20* (1), 11–30. https://doi.org/10.5217/ir.2020.00155.

(26) Hanoodi, M.; Mittal, M. Methotrexate. In *StatPearls*; StatPearls Publishing: Treasure Island (FL), 2023.

(27) Naganuma, M.; Fujii, T.; Watanabe, M. The Use of Traditional and Newer Calcineurin Inhibitors in Inflammatory Bowel Disease. *J. Gastroenterol.* 2011, *46* (2), 129–137. https://doi.org/10.1007/s00535-010-0352-z.

(28) Olivera, P.; Danese, S.; Peyrin-Biroulet, L. JAK Inhibition in Inflammatory Bowel Disease. *Expert Rev. Clin. Immunol.* 2017, *13* (7), 693–703. https://doi.org/10.1080/1744666X.2017.1291342.

(29) Chan, H. C.; Ng, S. C. Emerging Biologics in Inflammatory Bowel Disease. *J. Gastroenterol.* 2017, *52* (2), 141–150. https://doi.org/10.1007/s00535-016-1283-0.

(30) Nielsen, O. H.; Ainsworth, M. A. Tumor Necrosis Factor Inhibitors for Inflammatory Bowel Disease. *N. Engl. J. Med.* 2013, *369* (8), 754–762. https://doi.org/10.1056/NEJMct1209614.

(31) Gubatan, J.; Keyashian, K.; Rubin, S. J. S.; Wang, J.; Buckman, C. A.; Sinha, S. Anti-Integrins for the Treatment of Inflammatory Bowel Disease: Current Evidence and

Perspectives. *Clin. Exp. Gastroenterol.* 2021, *14*, 333–342. https://doi.org/10.2147/CEG.S293272.

(32) Justiz Vaillant, A. A.; Qurie, A. Interleukin. In *StatPearls*; StatPearls Publishing: Treasure Island (FL), 2024.

(33) Justiz Vaillant, A. A.; Qurie, A. Interleukin. In *StatPearls*; StatPearls Publishing: Treasure Island (FL), 2023.

(34) Gisbert, J. P.; Chaparro, M.; Gomollón, F. Common Misconceptions about 5-Aminosalicylates and Thiopurines in Inflammatory Bowel Disease. *World J. Gastroenterol. WJG* 2011, *17* (30), 3467–3478. https://doi.org/10.3748/wjg.v17.i30.3467.

(35) Hu, B.; Zhong, L.; Weng, Y.; Peng, L.; Huang, Y.; Zhao, Y.; Liang, X.-J. Therapeutic siRNA: State of the Art. *Signal Transduct. Target. Ther.* 2020, *5* (1), 1–25. https://doi.org/10.1038/s41392-020-0207-x.

(36) Chevalier, R. siRNA Targeting and Treatment of Gastrointestinal Diseases. *Clin. Transl. Sci.* 2019, *12* (6), 573–585. https://doi.org/10.1111/cts.12668.

(37) Ahn, I.; Kang, C. S.; Han, J. Where Should siRNAs Go: Applicable Organs for siRNA Drugs. *Exp. Mol. Med.* 2023, *55* (7), 1283–1292. https://doi.org/10.1038/s12276-023-00998-y.

(38) Traber, G. M.; Yu, A.-M. RNAi-Based Therapeutics and Novel RNA Bioengineering Technologies. *J. Pharmacol. Exp. Ther.* 2023, *384* (1), 133–154. https://doi.org/10.1124/jpet.122.001234.

(39) Shinn, J.; Lee, J.; Lee, S. A.; Lee, S. J.; Choi, A. H.; Kim, J. S.; Kim, S. J.; Kim, H. J.; Lee, C.; Kim, Y.; Kim, J.; Choi, J.; Jung, B.; Kim, T.; Nam, H.; Kim, H.; Lee, Y. Oral Nanomedicines for siRNA Delivery to Treat Inflammatory Bowel Disease. *Pharmaceutics*

2022, *14* (9), 1969. https://doi.org/10.3390/pharmaceutics14091969.

(40) Tokatlian, T.; Segura, T. siRNA Applications in Nanomedicine. *WIREs Nanomedicine Nanobiotechnology* 2010, *2* (3), 305–315. https://doi.org/10.1002/wnan.81.

(41) Ball, R. L.; Bajaj, P.; Whitehead, K. A. Oral Delivery of siRNA Lipid Nanoparticles: Fate in the GI Tract. *Sci. Rep.* 2018, *8* (1), 2178. https://doi.org/10.1038/s41598-018-20632-6.

(42) Sajid, M. I.; Moazzam, M.; Kato, S.; Yeseom Cho, K.; Tiwari, R. K. Overcoming Barriers for siRNA Therapeutics: From Bench to Bedside. *Pharmaceuticals* 2020, *13* (10), 294. https://doi.org/10.3390/ph13100294.

(43) Shajari, N.; Mansoori, B.; Davudian, S.; Mohammadi, A.; Baradaran, B. Overcoming the Challenges of siRNA Delivery: Nanoparticle Strategies. *Curr. Drug Deliv.* 2017, *14* (1), 36–46.

(44) Mitchell, M. J.; Billingsley, M. M.; Haley, R. M.; Wechsler, M. E.; Peppas, N. A.; Langer, R. Engineering Precision Nanoparticles for Drug Delivery. *Nat. Rev. Drug Discov.* 2021, *20* (2), 101–124. https://doi.org/10.1038/s41573-020-0090-8.

(45) Mainini, F.; Eccles, M. R. Lipid and Polymer-Based Nanoparticle siRNA Delivery Systems for Cancer Therapy. *Molecules* 2020, *25* (11), 2692. https://doi.org/10.3390/molecules25112692.

(46) Mahmoodi Chalbatani, G.; Dana, H.; Gharagouzloo, E.; Grijalvo, S.; Eritja, R.; Logsdon, C. D.; Memari, F.; Miri, S. R.; Rad, M. R.; Marmari, V. Small Interfering RNAs (siRNAs) in Cancer Therapy: A Nano-Based Approach. *Int. J. Nanomedicine* 2019, *14*, 3111–3128. https://doi.org/10.2147/IJN.S200253.

(47) Padda, I. S.; Mahtani, A. U.; Parmar, M. Small Interfering RNA (siRNA) Therapy. In *StatPearls*; StatPearls Publishing: Treasure Island (FL), 2023.

(48) Yi Xue, H.; Guo, P.; Wen, W.-C.; Lun Wong, H. Lipid-Based Nanocarriers for RNA Delivery. *Curr. Pharm. Des.* 2015, *21* (22), 3140–3147.

(49) Knipe, J. M.; Strong, L. E.; Peppas, N. A. Enzyme- and pH-Responsive Microencapsulated Nanogels for Oral Delivery of siRNA to Induce TNF-α Knockdown in the Intestine. *Biomacromolecules* 2016, *17* (3), 788–797. https://doi.org/10.1021/acs.biomac.5b01518.

(50) Liechty, W. B.; Scheuerle, R. L.; Vela Ramirez, J. E.; Peppas, N. A. Cytoplasmic Delivery of Functional siRNA Using pH-Responsive Nanoscale Hydrogels. *Int. J. Pharm.* 2019, *562*, 249–257. https://doi.org/10.1016/j.ijpharm.2019.03.013.

(51) Notabi, M. K.; Arnspang, E. C.; Peppas, N. A.; Andersen, M. Ø. siRNA Delivery Mediated by pH and Redox Responsive p(DEAEMA-Co-HEMA-g-PEGMA) Nanogels. *J. Drug Deliv. Sci. Technol.* 2023, *86*, 104510. https://doi.org/10.1016/j.jddst.2023.104510.

(52) Verma, P.; Srivastava, A.; Srikanth, C. V.; Bajaj, A. Nanoparticle-Mediated Gene Therapy Strategies for Mitigating Inflammatory Bowel Disease. *Biomater. Sci.* 2021, *9* (5), 1481–1502. https://doi.org/10.1039/D0BM01359E.

(53) Jayaraman, M.; Ansell, S. M.; Mui, B. L.; Tam, Y. K.; Chen, J.; Du, X.; Butler, D.; Eltepu, L.; Matsuda, S.; Narayanannair, J. K.; Rajeev, K. G.; Hafez, I. M.; Akinc, A.; Maier, M. A.; Tracy, M. A.; Cullis, P. R.; Madden, T. D.; Manoharan, M.; Hope, M. J. Maximizing the Potency of siRNA Lipid Nanoparticles for Hepatic Gene Silencing In Vivo. *Angew. Chem. Int. Ed Engl.* 2012, *51* (34), 8529–8533. https://doi.org/10.1002/anie.201203263.

(54) Fairman, K.; Li, M.; Ning, B.; Lumen, A. Physiologically Based Pharmacokinetic (PBPK) Modeling of RNAi Therapeutics: Opportunities and Challenges. *Biochem. Pharmacol.* 2021, *189*, 114468. https://doi.org/10.1016/j.bcp.2021.114468.

(55) Currie, G. M. Pharmacology, Part 2: Introduction to Pharmacokinetics. *J. Nucl. Med.*

Technol. 2018, *46* (3), 221–230. https://doi.org/10.2967/jnmt.117.199638.

(56) Meibohm, B.; Derendorf, H. Basic Concepts of Pharmacokinetic/Pharmacodynamic (PK/PD) Modeling. *Int. J. Clin. Pharmacol. Ther.* 1997, *35*, 401–413.

(57) Jones, H.; Chen, Y.; Gibson, C.; Heimbach, T.; Parrott, N.; Peters, S.; Snoeys, J.; Upreti, V.; Zheng, M.; Hall, S. Physiologically Based Pharmacokinetic Modeling in Drug Discovery and Development: A Pharmaceutical Industry Perspective. *Clin. Pharmacol. Ther.* 2015, *97* (3), 247–262. https://doi.org/10.1002/cpt.37.

(58) Jones, H.; Rowland-Yeo, K. Basic Concepts in Physiologically Based Pharmacokinetic Modeling in Drug Discovery and Development. *CPT Pharmacomet. Syst. Pharmacol.* 2013, *2* (8), e63. https://doi.org/10.1038/psp.2013.41.

(59) Jing, X.; Arya, V.; Reynolds, K. S.; Rogers, H. Clinical Pharmacology of RNA Interference–Based Therapeutics: A Summary Based on Food and Drug Administration–Approved Small Interfering RNAs. *Drug Metab. Dispos.* 2023, *51* (2), 193–198. https://doi.org/10.1124/dmd.122.001107.

(60) Jo, S. J.; Chae, S. U.; Lee, C. B.; Bae, S. K. Clinical Pharmacokinetics of Approved RNA Therapeutics. *Int. J. Mol. Sci.* 2023, *24* (1), 746. https://doi.org/10.3390/ijms24010746.

(61) May Zhang, M.; Bahal, R.; Rasmussen, T. P.; Manautou, J. E.; Zhong, X. The Growth of siRNA-Based Therapeutics: Updated Clinical Studies. *Biochem. Pharmacol.* 2021, *189*, 114432. https://doi.org/10.1016/j.bcp.2021.114432.

(62) Park, J.; Park, J.; Pei, Y.; Xu, J.; Yeo, Y. Pharmacokinetics and Biodistribution of Recently-Developed siRNA Nanomedicines. *Adv. Drug Deliv. Rev.* 2016, *104*, 93–109. https://doi.org/10.1016/j.addr.2015.12.004.

(63) Sahay, G.; Querbes, W.; Alabi, C.; Eltoukhy, A.; Sarkar, S.; Zurenko, C.; Karagiannis, E.;

Love, K.; Chen, D.; Zoncu, R.; Buganim, Y.; Schroeder, A.; Langer, R.; Anderson, D. G. Efficiency of siRNA Delivery by Lipid Nanoparticles Is Limited by Endocytic Recycling. *Nat. Biotechnol.* 2013, *31* (7), 653–658. https://doi.org/10.1038/nbt.2614.

(64) Attarwala, H. Z.; Suri, K.; Amiji, M. M. Pharmacokinetics and Biodistribution Analysis of Small Interference RNA for Silencing Tissue Transglutaminase-2 in Celiac Disease After Oral Administration in Mice Using Gelatin-Based Multicompartmental Delivery Systems. *Bioelectricity* 2020, *2* (2), 167–174. https://doi.org/10.1089/bioe.2020.0008.

(65) Han, L.; Tang, C.; Yin, C. Oral Delivery of shRNA and siRNA via Multifunctional Polymeric Nanoparticles for Synergistic Cancer Therapy. *Biomaterials* 2014, *35* (15), 4589–4600. https://doi.org/10.1016/j.biomaterials.2014.02.027.

(66) Kang, S. H.; Revuri, V.; Lee, S.-J.; Cho, S.; Park, I.-K.; Cho, K. J.; Bae, W. K.; Lee, Y.-K. Oral siRNA Delivery to Treat Colorectal Liver Metastases. *ACS Nano* 2017, *11* (10), 10417–10429. https://doi.org/10.1021/acsnano.7b05547.

(67) Hack, C. E.; Efremenko, A. Y.; Pendse, S. N.; Ellison, C. A.; Najjar, A.; Hewitt, N.; Schepky, A.; Clewell, H. J. Chapter 4 - Physiologically Based Pharmacokinetic Modeling Software. In *Physiologically Based Pharmacokinetic (PBPK) Modeling*; Fisher, J. W., Gearhart, J. M., Lin, Z., Eds.; Academic Press, 2020; pp 81–126. https://doi.org/10.1016/B978-0-12-818596-4.00004-7.

(68) Lin, Z.; Jaberi-Douraki, M.; He, C.; Jin, S.; Yang, R. S. H.; Fisher, J. W.; Riviere, J. E. Performance Assessment and Translation of Physiologically Based Pharmacokinetic Models From acslX to Berkeley Madonna, MATLAB, and R Language: Oxytetracycline and Gold Nanoparticles As Case Examples. *Toxicol. Sci.* 2017, *158* (1), 23–35. https://doi.org/10.1093/toxsci/kfx070.

(69) Vasić, V.; Gustafsson, J.; Nowshahr, E. Y.; Stenvall, A.; Beer, A. J.; Gleisner, K. S.; Glatting, G. A PBPK Model for PRRT with [177Lu]Lu-DOTA-TATE: Comparison of Model Implementations in SAAM II and MATLAB/SimBiology. *Phys. Med.* 2024, *119*, 103299. https://doi.org/10.1016/j.ejmp.2024.103299.

(70) *SimBiology*. https://www.mathworks.com/products/simbiology.html (accessed 2024-03-19).

(71) Yu, X.; Xiao, H.; Muqier, M.; Han, S.; Baigude, H. Effect of the Array of Amines on the Transfection Efficiency of Cationic Peptidomimetic Lipid Molecules into Neural Cells. *RSC Adv.* 2022, *12* (33), 21567–21573. https://doi.org/10.1039/D2RA03347J.

(72) Hall, C.; Lueshen, E.; Mošat', A.; Linninger, A. A. Interspecies Scaling in Pharmacokinetics: A Novel Whole-Body Physiologically Based Modeling Framework to Discover Drug Biodistribution Mechanisms *in Vivo*. *J. Pharm. Sci.* 2012, *101* (3), 1221–1241. https://doi.org/10.1002/jps.22811.

(73) *Surface area assessment of the murine intestinal tract as a prerequisite for oral dose translation from mouse to man - C Casteleyn, A Rekecki, A Van Der Aa, P Simoens, W Van Den Broeck, 2010*. https://journals.sagepub.com/doi/10.1258/la.2009.009112 (accessed 2024-03-24).

(74) McConnell, E. L.; Basit, A. W.; Murdan, S. Measurements of Rat and Mouse Gastrointestinal pH, Fluid and Lymphoid Tissue, and Implications for in-Vivo Experiments. *J. Pharm. Pharmacol.* 2008, *60* (1), 63–70. https://doi.org/10.1211/jpp.60.1.0008.

(75) Shah, D. K.; Betts, A. M. Towards a Platform PBPK Model to Characterize the Plasma and Tissue Disposition of Monoclonal Antibodies in Preclinical Species and Human. *J. Pharmacokinet. Pharmacodyn.* 2012, *39* (1), 67–86. https://doi.org/10.1007/s10928-011-9232-2.

(76) Altaf, S.; Kaleem, A.; Fatima, S. K.; Sabir, A.; Khan, I. Determination of Pharmacokinetic Parameters by the Application of Noncompartmental Analysis. *Glob. Pharm. Sci. Rev.* 2018, *II* (I), 42–47. https://doi.org/10.31703/gpsr.2017(II-I).05.

(77) *Noncompartmental Analysis - MATLAB & Simulink*. https://www.mathworks.com/help/simbio/ug/non-compartmental-analysis.html (accessed 2024-03-24).

(78) Ayyar, V. S.; Song, D.; Zheng, S.; Carpenter, T.; Heald, D. L. Minimal Physiologically Based Pharmacokinetic-Pharmacodynamic (mPBPK-PD) Model of N-Acetylgalactosamine–Conjugated Small Interfering RNA Disposition and Gene Silencing in Preclinical Species and Humans. *J. Pharmacol. Exp. Ther.* 2021, *379* (2), 134–146. https://doi.org/10.1124/jpet.121.000805.

(79) Bartlett, D. W.; Davis, M. E. Insights into the Kinetics of siRNA-Mediated Gene Silencing from Live-Cell and Live-Animal Bioluminescent Imaging. *Nucleic Acids Res.* 2006, *34* (1), 322–333. https://doi.org/10.1093/nar/gkj439.

(80) LARAUCHE, M.; KIANK, C.; TACHE, Y. CORTICOTROPIN RELEASING FACTOR SIGNALING IN COLON AND ILEUM: REGULATION BY STRESS AND PATHOPHYSIOLOGICAL IMPLICATIONS. *J. Physiol. Pharmacol.* 2009, *60* (Suppl 7), 33–46.

(81) *What is inflammatory bowel disease (IBD)? | IBD*. https://www.cdc.gov/ibd/what-is-IBD.htm (accessed 2024-04-22).

(82) *Inflammatory Bowel Disease (IBD)*. https://www.hopkinsmedicine.org/health/conditions-and-diseases/inflammatory-bowel-disease (accessed 2024-04-22).

(83) *Global Sensitivity Analysis with SimBiology*. https://www.mathworks.com/videos/global-sensitivity-analysis-with-simbiology-1596700380846.html (accessed 2024-04-07).

(84) Liu, D.; Li, L.; Rostami-Hodjegan, A.; Bois, F. Y.; Jamei, M. Considerations and Caveats When Applying Global Sensitivity Analysis Methods to Physiologically Based Pharmacokinetic Models. *AAPS J.* 2020, *22* (5), 93. https://doi.org/10.1208/s12248-020-00480-x.

BIOGRAPHY

Ravali Bhavaraju is graduating from The University of Texas at Austin with a B.S. in Biomedical Engineering and a B.A. in Plan II Honors. At UT, she was involved with the Women in Engineering Program and Texas Women of Excellence, and she has previously completed summer internships with Eli Lilly and Company and Stryker. She joined Dr. Peppas' laboratory in Fall 2023 to research physiologically based pharmacokinetic modeling of siRNA for Inflammatory Bowel Disease. After graduation, Ravali will be joining Emerson in their Engineers in Leadership Program.